



# Catalytic oxidation of dimethyl disulfide ( $\text{CH}_3\text{SSCH}_3$ ) over monometallic Au, Pt and Cu catalysts supported on $\gamma\text{-Al}_2\text{O}_3$ , $\text{CeO}_2$ and $\text{CeO}_2\text{-Al}_2\text{O}_3$

Tuomas K. Nevanperä<sup>a,\*</sup>, Satu Ojala<sup>a</sup>, Nicolas Bion<sup>b</sup>, Florence Epron<sup>b</sup>, Riitta L. Keiski<sup>a</sup>

<sup>a</sup> University of Oulu, Faculty of Technology, Environmental and Chemical Engineering, FI-90014 University of Oulu, P.O. Box 4300, Finland

<sup>b</sup> Université de Poitiers, CNRS UMR 7285, Institut de Chimie des Milieux et Matériaux de Poitiers (IC2MP), 4 rue Michel Brunet, TSA 51106, 86073 Poitiers Cedex 9, France

## ARTICLE INFO

### Article history:

Received 29 May 2015

Received in revised form 5 October 2015

Accepted 6 October 2015

Available online 14 October 2015

### Keywords:

Emission abatement

Volatile organic compound

Sulfur

Activity

Stability

## ABSTRACT

Au, Cu, and Pt catalysts supported on  $\text{Al}_2\text{O}_3$ ,  $\text{CeO}_2$ , and  $\text{CeO}_2\text{-Al}_2\text{O}_3$  were investigated in the oxidation of  $\text{CH}_3\text{SSCH}_3$ . The  $\text{H}_2$ -TPR experiments indicated that the improved reducibility has a key role in  $\text{CH}_3\text{SSCH}_3$  oxidation. In addition, oxygen activation showed correlation with the oxidation product formation. With Cu containing catalysts the oxidation reaction of  $\text{CH}_3\text{SSCH}_3$  started at lower temperatures independent of the support. In addition, the presence of Cu as well as  $\text{CeO}_2$  resulted in significant production of formaldehyde instead of  $\text{CO}_2$ . Pt catalysts showed a significant decline in  $\text{SO}_2$  formation at high temperature showing over-oxidation or potential to deactivation when supported on  $\text{Al}_2\text{O}_3$  and  $\text{CeO}_2\text{-Al}_2\text{O}_3$ . Stability test of Au/ $\text{CeO}_2\text{-Al}_2\text{O}_3$  for more than 40 h showed that the catalyst is durable but its selectivity should be enhanced further.

© 2015 Elsevier B.V. All rights reserved.

## 1. Introduction

The extension of industrial activities and the mass production of chemicals result in an enormous array of emissions of different chemical compounds that can be destructive to the environment and human health. Emissions of volatile organic compounds (VOC) have been regulated by strict EU legislation for years due to their harmful/damaging effects. The recast of the IPPC (Integrated pollution prevention and control) Directive tighten up the previous VOC Directive (1999) by introducing measures to implement BAT (Best available technique) for emission abatement [1,2]. Referring to the Gothenburg protocol designed to reduce acidification, eutrophication and ground-level ozone by setting emission ceilings for air pollutants, EU member countries must jointly cut their emissions of VOCs by 28% between 2005 and 2020 [3].

Volatile organic compounds (VOCs) are one of the main contributors causing direct (toxicity, odor) and indirect (smog formation) air pollution. They are also classed as greenhouse gases (GHG) and their GHG effects can be more than 50 times higher than the effect of  $\text{CO}_2$ . Thiols, disulfides, and other organosulfur com-

pounds are present in virtually all hydrocarbon feedstocks [4]. Sulfur containing VOCs (SVOCs) are originating especially from wood-industry, such as pulping processes and chemical production, landfill sites and wastewater treatment plants. Examples of SVOCs are compounds such as methyl mercaptan ( $\text{CH}_3\text{SH}$ ), dimethyl sulfide ( $\text{CH}_3\text{SCH}_3$ ) and dimethyl disulfide ( $\text{CH}_3\text{SSCH}_3$ ).

Mercaptans and dimethyl sulfides are not extremely toxic, but they can be repulsively malodorous even at very low concentrations causing discomfort in urban areas and therefore they require highly efficient treatment methods [5]. The occurrence of sulfides is found in natural products or materials derived from biological origin, such as petroleum. Alkyl sulfides are often formed as secondary products in industrial processes such as by-products in the sulfite pulp process [6]. Low-molecular-weight alkyl disulfides have been found in crude benzene, synthesis gas, and Kraft pulp digester exhaust gas [7].

Catalytic abatement is applicable especially when emission mixtures are complicated and when the total VOC concentrations vary from low to high. Catalytic oxidation is environmentally sound and even more economically feasible when processes using reverse-flow-reactors (RFR) are used. The application of catalytic incineration to SVOC oxidation is a tempting possibility due to its high energy and purification efficiencies, but certain aspects *i.e.*,

\* Corresponding author. Fax: +358 8 5534112.

E-mail address: [tuomas.nevanpera@oulu.fi](mailto:tuomas.nevanpera@oulu.fi) (T.K. Nevanperä).

selectivity, activity and stability, related to the catalysts need still to be improved [8].

A majority of the catalysts used for the VOC abatement consists of noble metals or base metal oxides. Catalysts containing noble metals, such as Pt, Pd and Rh, can suffer from poisoning by sulfur compounds and are not directly the best candidates for the SVOC treatment [9]. Sulfur is a well-known catalyst poison, but the poisoning can be reversible and depends on temperature [5,8,10–13]. Several possible deactivation mechanisms due to sulfurous compounds have been found.  $\text{CH}_3\text{SH}$ ,  $\text{CH}_3\text{SCH}_3$ ,  $\text{CH}_3\text{SSCH}_3$  and  $\text{H}_2\text{S}$  can adsorb on the surface of catalyst resulting in poisoning. During the oxidation reactions the described compounds can also cause severe sulfating of the catalyst when  $\text{SO}_2$  is formed and further oxidized to  $\text{SO}_3$ , which reacts with the support. Furthermore,  $\text{SO}_2$  can decompose either spontaneously or by thermal activation on the metal substrates (Fe, Ni, Cu, Mo, Ru, Rh, Pt, Zb, Sn, Cs) except on Ag. In addition, it has been shown that  $\text{SO}_2$  can react with Pt(111) at room temperature, leading to elemental S deposition and the formation of  $\text{SO}_3$  and  $\text{SO}_4$  species on the surface of the metal. The molecular  $\text{SO}_x$  species dissociate when heated up to 450 K and thus deposit S adatoms [14]. Moreover,  $\text{H}_2\text{S}$  may react to form metal sulfides, which is an irreversible reaction. The by-product in oxidation reactions of SVOCs ( $\text{SO}_3$ ) may react with water to form sulfuric acid, which is inevitably hazardous for catalysts and process equipment surfaces [8,10,15–20].

The earliest studies of gaseous oxidation of alkane thiols and  $\text{CH}_3\text{SSCH}_3$  were done by Cullis and Roselaar [21,22]. They found that the principal products of the gaseous oxidation of  $\text{CH}_3\text{SSCH}_3$  are  $\text{SO}_2$ ,  $\text{CO}_2$ ,  $\text{CO}$ , and  $\text{CH}_2\text{OH}$ . Formaldehyde ( $\text{CH}_2\text{O}$ ) and methyl mercaptan ( $\text{CH}_3\text{SH}$ ) are apparently formed as intermediates. Wang and Weng [11] studied the activity of eight different metal oxides ( $\text{Co}_3\text{O}_4$ ,  $\text{ZnO}$ ,  $\text{NiO}$ ,  $\text{MnO}_2$ ,  $\text{Fe}_2\text{O}_3$ ,  $\text{Cr}_2\text{O}_3$ ,  $\text{MoO}_3$ ,  $\text{CuO}$ ) supported on  $\gamma\text{-Al}_2\text{O}_3$  in the oxidation of  $\text{CH}_3\text{SSCH}_3$ . From these,  $\text{CuO-Al}_2\text{O}_3$  showed the best activity. In the same study the effect of the promoter metal on  $\text{CuO-Al}_2\text{O}_3$  was investigated by loading  $\text{CuO-Al}_2\text{O}_3$  with nine different metal oxides ( $\text{Co}_3\text{O}_4$ ,  $\text{ZnO}$ ,  $\text{NiO}$ ,  $\text{MnO}_2$ ,  $\text{Fe}_3\text{O}_4$ ,  $\text{Cr}_2\text{O}_3$ ,  $\text{SrO}$ ,  $\text{La}_2\text{O}_3$ ,  $\text{MoO}_3$ ). Conversion of  $\text{CH}_3\text{SSCH}_3$  and yield of  $\text{CO}_2$  were observed to be at highest when Mo was added as a promoter. Ojala [23] conducted experiments with different Pt and Pd containing catalysts supported on  $\text{Al}_2\text{O}_3$  as well as  $\text{MnO}_2\text{-MgO}$ ,  $\text{Cu}_x\text{Mg}_{(1-x)}\text{Cr}_2\text{O}_4$  and  $\text{Cu}_x\text{Cr}_2\text{O}_4$  in the oxidation of  $\text{CH}_3\text{SH}$  and  $\text{CH}_3\text{SSCH}_3$ . Catalytic activities of noble metals in the  $\text{CH}_3\text{SSCH}_3$  oxidation were not notably different. Kastner et al. [24] used coal and wood fly ash as catalysts in the oxidation reaction of  $\text{H}_2\text{S}$ ,  $\text{CH}_3\text{SCH}_3$ ,  $\text{CH}_3\text{SSCH}_3$ , and  $\text{CH}_3\text{CH}_2\text{SH}$ . Fly ash can catalyze the oxidation of  $\text{H}_2\text{S}$  and  $\text{CH}_3\text{CH}_2\text{SH}$  but not  $\text{CH}_3\text{SCH}_3$  and  $\text{CH}_3\text{SSCH}_3$  at room temperature.

According to recent discoveries gold as small particles (<5 nm) supported on certain oxide supports exhibit surprisingly high catalytic activity for different oxidation reactions [25,26]. More recently the activity of supported gold nanoparticles for the application of VOC treatment has drawn considerable interest. Various authors have reported the catalytic performance of Au nanoparticles for example on  $\text{Fe}_2\text{O}_3$ ,  $\text{Co}_2\text{O}_3$ ,  $\text{MnO}_2$ ,  $\text{NiO}$ , and  $\text{CeO}_2$  [27–31]. These papers indicate that Au catalysts can overcome the performance of conventionally used  $\text{Pt/Al}_2\text{O}_3$ . However, only a few authors have investigated the possibility to use gold catalysts in the oxidation of SVOCs. Kucherov et al. [32,33] studied the removal of  $\text{CH}_3\text{OH}$ ,  $\text{CH}_3\text{SH}$ , and  $\text{CH}_3\text{SSCH}_3$  from air using  $\text{Au/HZSM-5}$  and  $\text{Au-Rh/HZSM-5}$  catalysts. The experiments demonstrated high activity and stability (sulfur-resistance) for the  $\text{Au-Rh/HZSM-5}$  catalyst at temperatures as low as 290 °C. A less active monometallic  $\text{Au/HZSM-5}$  also provides an effective and stable oxidative removal of VOC and SVOC at 500 °C. Ojala et al. [34] investigated Au-based catalysts in the abatement of TRS emissions. The catalysts were supported on pulverized or pelletized  $\text{Al}_2\text{O}_3$  powder (AIP) and a knitted

activated carbon cloth (Kynol TM). The complete conversion of  $\text{CH}_3\text{SSCH}_3$  over both pelletized catalysts 2.7Au/AIP and 3.6Au/AIP were achieved at around 500 °C [34].

Sulfur forms stable compounds with all the transition metals. For example the reaction between sulfur and copper gives  $\text{CuS}$  and  $\text{Cu}_2\text{S}$ . In the case of Pt, sulfur withdraws a charge from the metal affecting valence bands, which can lead to significant changes in the catalytic properties. Interestingly, the interaction between sulfur and Au is poor. Au shows the lowest reactivity towards sulfur among transition and noble metals. Usually the chemical bonds between sulfur and metals are strong [14]. From this perspective, Au has a high electronegativity, and consequently Au does not react readily with other electronegative elements such as sulfur or oxygen [25].

As previously mentioned, in SVOC oxidation Pt catalysts can oxidize the desired product, i.e.,  $\text{SO}_2$  further to  $\text{SO}_3$ . The formed  $\text{SO}_3$  may further react with the catalyst to form sulfides and sulfates, and with moisture it can react to sulfuric acid that can also react with the catalyst, and in addition with the construction materials of the incinerator [23]. The possible replacement or additive to a Pt-based catalyst is Cu. Cu catalysts are active in  $\text{CH}_3\text{SSCH}_3$  oxidation and resist sulfur to some degree [11]. However, sensitivity of copper catalysts to sulfur poisoning is severe and pronounced. Copper reacting with  $\text{SO}_2$  or other sulfur-containing compounds causing corrosion is a major problem [14]. From the perspective of activity, Au catalysts have shown promising results in terms of complete conversion of  $\text{CH}_3\text{SSCH}_3$  at low temperatures [34].

In this study nine different monometallic Au, Pt, and Cu catalysts were examined in catalytic oxidation of  $\text{CH}_3\text{SSCH}_3$  using Cu and Pt catalysts as references. The objective was to compare the activity and selectivity of the catalysts and in addition to study if gold is a stable catalyst in the  $\text{CH}_3\text{SSCH}_3$  oxidation.

## 2. Experimental

### 2.1. Catalyst preparation

Three different support oxides ( $\text{Al}_2\text{O}_3$ ,  $\text{CeO}_2$  and  $\text{CeO}_2\text{-Al}_2\text{O}_3$  containing 20 wt.% of  $\text{CeO}_2$ ) were used in the preparation of nine monometallic catalysts. Nomenclature and desired compositions of the catalysts are described in Table 1.

Commercial aluminum oxide ( $\gamma\text{-Al}_2\text{O}_3$ , Rhodia) was used in the preparation of catalyst support containing 20 wt.% of  $\text{CeO}_2$  by wet impregnation in excess solution [35]. The metal salt used for the impregnation was cerium (III) chloride heptahydrate ( $\text{CeCl}_3 \cdot 7\text{H}_2\text{O}$ , Acros Organics, 99%). The requisite amount of the metal salt was dissolved in distilled water (~25 mL) and mixed with 4 g of  $\gamma\text{-Al}_2\text{O}_3$  in a rotary evaporator in order to have 5 g of the  $\text{CeO}_2\text{-Al}_2\text{O}_3$  support. Next the solution was stirred vigorously for 2 h at room temperature. Evaporation of excess water was completed in a rotary evaporator at 60 °C. The obtained support material was dried further in an oven overnight at 120 °C.

Catalysts containing 5 wt.% of copper or 1 wt.% of platinum on commercial  $\gamma\text{-Al}_2\text{O}_3$  (Rhodia), commercial  $\text{CeO}_2$  (Rhodia) and  $\text{CeO}_2\text{-Al}_2\text{O}_3$  were prepared by wet impregnation. First the  $\gamma\text{-Al}_2\text{O}_3$  powder was wetted by distilled water in a beaker in order to have high dispersion and to maximize the mass transfer of added metal salts on the surface and the pores of the catalyst. The requisite quantity of metal salt ( $\text{Cu}(\text{NO}_3)_2 \cdot 3\text{H}_2\text{O}$ , Prolabo, 99% or  $\text{H}_2\text{PtCl}_6 \cdot 6\text{H}_2\text{O}$ , Alfa Aesar, Pt ca 38–40%) was dissolved in ~20 mL of distilled water. The solutions were mixed together and stirred for 18 h at room temperature. Finally the solution was dried on a sand bed at 60 °C and further in an oven at 120 °C overnight. Similar procedure was used in the preparation of  $\text{CeO}_2$  and  $\text{CeO}_2\text{-Al}_2\text{O}_3$  supported catalysts.

**Table 1**

Overview of the prepared catalysts with their desired compositions.

Catalyst abbreviation	Support	Metal	Amount of metal [wt.%]	Preparation method
Au/Al	Al <sub>2</sub> O <sub>3</sub>	Gold	1	Deposition-precipitation
Pt/Al	Al <sub>2</sub> O <sub>3</sub>	Platinum	1	Wet impregnation
Cu/Al	Al <sub>2</sub> O <sub>3</sub>	Copper	5	Wet impregnation
Au/Ce	CeO <sub>2</sub>	Gold	1	Deposition-precipitation
Pt/Ce	CeO <sub>2</sub>	Platinum	1	Wet impregnation
Cu/Ce	CeO <sub>2</sub>	Copper	5	Wet impregnation
Au/Ce-Al	CeO <sub>2</sub> -Al <sub>2</sub> O <sub>3</sub>	Gold	1	Deposition-precipitation
Pt/Ce-Al	CeO <sub>2</sub> -Al <sub>2</sub> O <sub>3</sub>	Platinum	1	Wet impregnation
Cu/Ce-Al	CeO <sub>2</sub> -Al <sub>2</sub> O <sub>3</sub>	Copper	5	Wet impregnation

Deposition-precipitation with urea was used as a preparation method for loading 1 wt.% of Au on the support according to the Ref. [35]. Support powder was first dispersed in distilled water. The temperature of the suspension was kept constant at 80 °C and agitated with a magnetic stirrer. Secondly, the requisite quantity of chloroauric acid (HAuCl<sub>4</sub>·3H<sub>2</sub>O, Acros) solution was added to the suspension and the temperature was let to stabilize. Thirdly, 4.5 g of urea (Aldrich, 99%) was added into the reactor vessel and the suspension was stirred continuously for 4 h. The four hours agitation time was chosen, since the deposition time of 4 h compared to 12 h did not have a major effect on the Au content nor the particle size according to Zanella et al. [36]. The reactor vessel was covered thoroughly with aluminum foil in order to avoid UV-light induced effects. The deposition was followed by centrifugation of the catalyst suspension in 50 mL tubes. The centrifugation was conducted three times. After the first and the second centrifugations separated water was decanted away and the tube was refilled with distilled water. After the following separation and washing, the solid was collected and moved to a rotary evaporator and dried at ~40 °C in a water bath under vacuum. Final drying was done in an oven at 120 °C overnight. During further handling and storage, exposure of samples to light was minimized. The samples were stored at room temperature and kept away from light.

Calcination temperature was chosen according to the application in which the total conversion of CH<sub>3</sub>SSCH<sub>3</sub> is achieved at around 600 °C [23]. All catalysts as well as the prepared CeO<sub>2</sub>-Al<sub>2</sub>O<sub>3</sub> support were calcined in 10 vol-% O<sub>2</sub>/N<sub>2</sub> flow by heating them from room temperature up to 600 °C with a heating rate of 5 °C min<sup>-1</sup> and dwelling at 600 °C for 5 h.

## 2.2. Catalyst characterization

All catalysts as well as supports were characterized using BET, ICP-OES, X-ray diffraction (XRD), temperature programmed reduction with hydrogen (H<sub>2</sub>-TPR), and temperature programmed isotopic exchange (TPIE) with labeled oxygen (<sup>18</sup>O<sub>2</sub>). In addition, X-Ray fluorescence (XRF) was used to verify the weight ratio between ceria and alumina in the prepared CeO<sub>2</sub>-Al<sub>2</sub>O<sub>3</sub> support.

Elemental compositions were determined using an ICP-OES equipment (PerkinElmer Optima 2000 DV or PerkinElmer Optima 5300 DV) after microwave-assisted aqua regia sample digestion.

PANalytical AXIOSmAX 4 kW PW2450 X-ray fluorescence spectrometer with Omnian application was used to deduce the weight ratio of ceria to alumina in the prepared CeO<sub>2</sub>-Al<sub>2</sub>O<sub>3</sub> support. The amount of 200 mg of CeO<sub>2</sub>-Al<sub>2</sub>O<sub>3</sub> was used for the preparation of fused bead for the analysis. Normalization to 100% was not used and no loss of ignition was taken into account, because the sample was calcined at 600 °C before preparing the fused bead.

The specific surface areas (S<sub>BET</sub>) were deduced from nitrogen adsorption at -196 °C performed with a Micromeritics Tristar 3000 apparatus. Prior to the measurements, the catalyst samples were pretreated at 250 °C under vacuum at least for 2 h in order to eliminate adsorbed compounds.

X-ray diffraction (XRD) was used to characterize the phase composition of the catalysts. The XRD patterns were recorded with a PANalytical Empyrean diffractometer using CuKα radiation (λ<sub>Kα1</sub> = 1.5406 Å) generated at 45 kV and 40 mA. The apparatus was equipped with a high-speed linear detector, X'Celerator, i.e., a silicon-based position-sensitive detector. The patterns were detected with the following specifications: step time 120 s, step 0.05°, linear detector length 0.5°.

H<sub>2</sub>-TPR was used to determine the reducibility of the catalysts. Before each H<sub>2</sub>-TPR experiment, the catalyst sample (200 mg) was pretreated *in situ* under an oxygen flow heating the sample from room temperature to 600 °C at a rate of 5 °C min<sup>-1</sup> and keeping it there for 10 min in order to eliminate residual species. Subsequently, the sample was cooled down to 35 °C under an oxygen flow in two steps. Oxygen was purged from the system under an argon flow during 10 min. Finally H<sub>2</sub>-TPR was carried out from 35 °C up to 400 °C. Water produced during the reduction was trapped from the exit of the reactor with magnesium perchlorate. Hydrogen consumption was followed using a thermal conductivity detector (TCD). H<sub>2</sub>-TPR data was treated with Origin 9.0 in order to identify peak positions.

Temperature programmed isotopic exchange (TPIE) experiments with labeled oxygen (<sup>18</sup>O<sub>2</sub>) were done in a closed-loop tubular quartz reactor. The setup is described in more detail in reference [37]. In order to minimize diffusion and mass transport effects causing differences on the partial pressures of different isotopomers in the system, oxygen was circulated in the reactor loop by a pump. The concentrations were measured continuously by a mass spectrometer (Pfeiffer Vacuum). Before each experiment the catalyst sample was oxidized *in-situ* by heating (10 °C min<sup>-1</sup>) from room temperature to 600 °C and keeping it there for 15 min followed by evacuation for 30 min. Next, the oven temperature was decreased to the starting level of the experiment (200 °C) while the catalyst sample was kept under vacuum. The experimental procedure was the following: the pre-determined amount of <sup>18</sup>O<sub>2</sub> (Isotec; 99.3 atom-% purity) was introduced into the system. The initial total pressure of the gas mixture was kept at a constant level (65 mbar) in all the experiments. The actual sample part of the reactor was sealed during the introduction of <sup>18</sup>O<sub>2</sub>. After measuring the initial concentrations of the gases at the beginning of the experiment, the reactor inlet was opened in order to initiate the reaction. During the exchange experiment temperature of the oven was increased from 200 °C to 600 °C with a heating rate of 2 °C min<sup>-1</sup>. The weight of the catalyst sample in each experiment was 20 mg.

High-resolution transmission electron microscope (HR-TEM) images were obtained using a JEOL JEM-2100 microscope with an accelerative voltage of 200 kV. The microscope was equipped with energy-dispersive X-ray spectroscopy (EDS).

## 2.3. Catalytic tests

The activities of the catalysts in the dimethyl disulfide (CH<sub>3</sub>SSCH<sub>3</sub>) oxidation were compared in terms of light-off curves

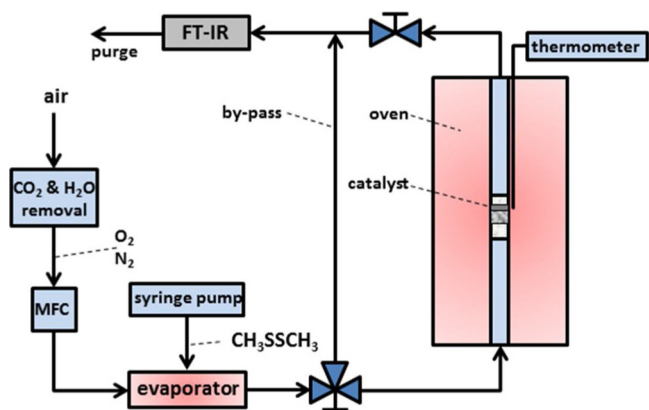


Fig. 1. An illustration of the reactor setup used for catalytic oxidation of  $\text{CH}_3\text{SSCH}_3$ .

derived from the data gained with a tubular quartz reactor working at atmospheric pressure with WHSV of  $720 \text{ g}_{\text{cat}}^{-1} \text{ h}^{-1}$ . A catalyst sample (100 mg) was placed in the reactor on the top of a quartz sand bed (400 mg) between two quartz wool plugs. Compressed air was cleaned from carbon dioxide and water by a gas cleaning unit, and fed into the system ( $1 \text{ dm}^3 \text{ min}^{-1}$ ). The liquid  $\text{CH}_3\text{SSCH}_3$  (Merck, >99%) was injected with a gas tight syringe into a vaporizer unit, which was heated up slightly over the boiling point of  $\text{CH}_3\text{SSCH}_3$  ( $>110^\circ\text{C}$ ) and the initial concentration during the experiment was set to 500 ppm. The furnace was heated from room temperature up to  $600^\circ\text{C}$  with a heating rate of  $5^\circ\text{C min}^{-1}$ . The analysis was done at ppm level by a multicomponent FTIR gas analyzer, Gasmet CR-2000, equipped with a liquid nitrogen cooled MCT-detector. The compounds analyzed were carbon dioxide, carbon monoxide, nitrogen monoxide, nitrogen dioxide, nitrous oxide, ammonia, sulfur dioxide, sulfur trioxide, methane, ethane, formaldehyde, methyl mercaptan, ethyl mercaptan, dimethyl sulfide, dimethyl disulfide, diethyl sulfate, carbonyl sulfite, ethylene, methanol, ethanol, formic acid, acetic acid, acetaldehyde, and acetone. Catalytic tests were conducted for all nine monometallic catalysts as well as for the corresponding supports. Each test was repeated at least once in order to validate the results. Due to the nature of the volatile and corrosive compounds, the setup is equipped with heated Teflon tubings ( $180^\circ\text{C}$ ) and acid resistant stainless steel connectors. A schematic illustration of the used setup is shown in Fig. 1.

Conversion of dimethyl disulfide (DMDS,  $\text{CH}_3\text{SSCH}_3$ ),  $\text{CO}_2$  yield,  $\text{SO}_2$  yield, and formaldehyde ( $\text{CH}_2\text{O}$ ) yield were calculated as follows:

$$X_{\text{DMDS}} [\%] = 100 \times \frac{C_{\text{DMDS}}^{\text{in}} - C_{\text{DMDS}}^{\text{out}}}{C_{\text{DMDS}}^{\text{in}}} \quad (1)$$

$$Y_x [\%] = 100 \times \frac{\dot{n}_x^{\text{out}}}{2 \times \dot{n}_{\text{DMDS}}^{\text{in}}} \quad (2)$$

where  $X$  is the conversion,  $Y$  is the yield,  $C$  is the concentration [ppm],  $\dot{n}$  is the molar flow rate [ $\text{mol min}^{-1}$ ], and  $x$  representing the compound ( $\text{CO}_2$ ,  $\text{SO}_2$ ,  $\text{CH}_2\text{O}$ ).

### 3. Results and discussion

#### 3.1. Characterization

Specific surface areas ( $S_{\text{BET}}$ ) and metal loadings of the prepared supports and catalysts are shown in Table 2. According to the characterization, the bare alumina support had a specific surface area ( $S_{\text{BET}}$ ) of  $100 \text{ m}^2 \text{ g}^{-1}$ . As expected, the  $S_{\text{BET}}$  value decreased due to the addition of ceria which is in accordance with the literature [35].

Table 2

Measured properties of the prepared catalysts.

Catalyst	$S_{\text{BET}}$ [ $\text{m}^2 \text{ g}^{-1}$ ] <sup>a</sup>	Metal loading [wt.%]
Au/Al	85	0.71
Pt/Al	85	1.10
Cu/Al	85	5.10
Au/Ce	240	0.93
Pt/Ce	190	1.12
Cu/Ce	210	5.60
Au/Ce-Al	75	0.46
Pt/Ce-Al	70	1.20
Cu/Ce-Al	70	5.80
Support		
Commercial $\text{Al}_2\text{O}_3$	100	–
Commercial $\text{CeO}_2$	200	–
$\text{CeO}_2\text{-Al}_2\text{O}_3$	65	Ce 14.3; Al 35.8

<sup>a</sup> Rounded values ( $\pm 5 \text{ m}^2 \text{ g}^{-1}$ ).

The  $\text{CeO}_2\text{-Al}_2\text{O}_3$  support had  $S_{\text{BET}}$  value of  $65 \text{ m}^2 \text{ g}^{-1}$  and the crystallite size of 20 nm. The elemental analyses by ICP-OES and XRF verified the desired weight ratio of 1:4 of ceria to alumina. ICP-OES gave 20.6 wt.% of ceria and 79.4 wt.% of alumina. XRF analysis showed 21.7 wt.% of  $\text{CeO}_2$  and 78.3 wt.% of  $\text{Al}_2\text{O}_3$  as well as trace amounts of chlorine in the sample as the indicative value, which is most probably due to the used precursor salt.

According to the ICP-OES results, the desired metal loadings were well achieved in the case of Pt and Cu impregnations (Table 2). The deposition of Au was not successful when  $\text{Al}_2\text{O}_3$  and  $\text{CeO}_2\text{-Al}_2\text{O}_3$  supported catalysts were considered. The amount of Au in the Au/Al catalyst was 0.71 wt.%, and in the Au/Ce-Al catalyst, only 0.46 wt.% of Au. The amount of Au found in the Au/Ce catalyst (0.93 wt.%) was close to that expected. In the case of Pt and Cu impregnated catalysts, the differences in actual loadings compared to the desired amounts are not as important as for the deposition of Au. The surface properties of alumina might have affected the deposition of Au, because the amount of Au was sufficient in the Au/Ce catalyst. This result could be explained by a change in pH during the reaction, which could be different depending on the support and on its ionic exchange capacity and point-zero charge (pzc). It was demonstrated that the deposition-precipitation of gold, and then the final gold content, depends strongly on the final pH of the solution [38].

$S_{\text{BET}}$  values of  $\text{Al}_2\text{O}_3$ -supported catalysts decreased from  $100 \text{ m}^2 \text{ g}^{-1}$  to approximately  $85 \text{ m}^2 \text{ g}^{-1}$  after the preparation procedure and the final calcination step (see Table 2). The differences are negligible, but can be noted. In the case of  $\text{CeO}_2$ -supported catalysts the  $S_{\text{BET}}$  values increased after the addition of Cu, the deposition of Au and the final calcination. However, the addition of Pt and the final calcination decreased the  $S_{\text{BET}}$  value slightly. Interestingly, and especially in the case of Au/Ce catalyst, the increase in the specific surface was noteworthy ( $\sim 40 \text{ m}^2 \text{ g}^{-1}$ ). The result was confirmed by repeated measurements. A similar effect was noticed by Tang et al. [39] who suggested the growth to be a consequence of two probable causes: either the addition of Au alone increased the specific surface area or the increase is a result of partial disruption of the  $\text{CeO}_2$  agglomerates, because Au is added in a highly acidic aqueous solution. Considering  $\text{CeO}_2\text{-Al}_2\text{O}_3$ -supported catalysts the addition of the metal on the surface increased the  $S_{\text{BET}}$  value by  $10 \text{ m}^2 \text{ g}^{-1}$ , at most. Altogether, the  $S_{\text{BET}}$  values of the  $\text{Al}_2\text{O}_3$ -supported and the  $\text{CeO}_2\text{-Al}_2\text{O}_3$ -supported catalysts did not differ substantially, since they were ranging from 70 to  $90 \text{ m}^2 \text{ g}^{-1}$ . Comparable  $S_{\text{BET}}$  values were desirable in further evaluation of the catalytic performance between the  $\text{Al}_2\text{O}_3$ -supported and the  $\text{CeO}_2\text{-Al}_2\text{O}_3$ -supported catalysts.

The XRD diffraction patterns for the prepared catalysts are shown in Fig. 2a–c. The diffraction peaks in the case of  $\text{Al}_2\text{O}_3$

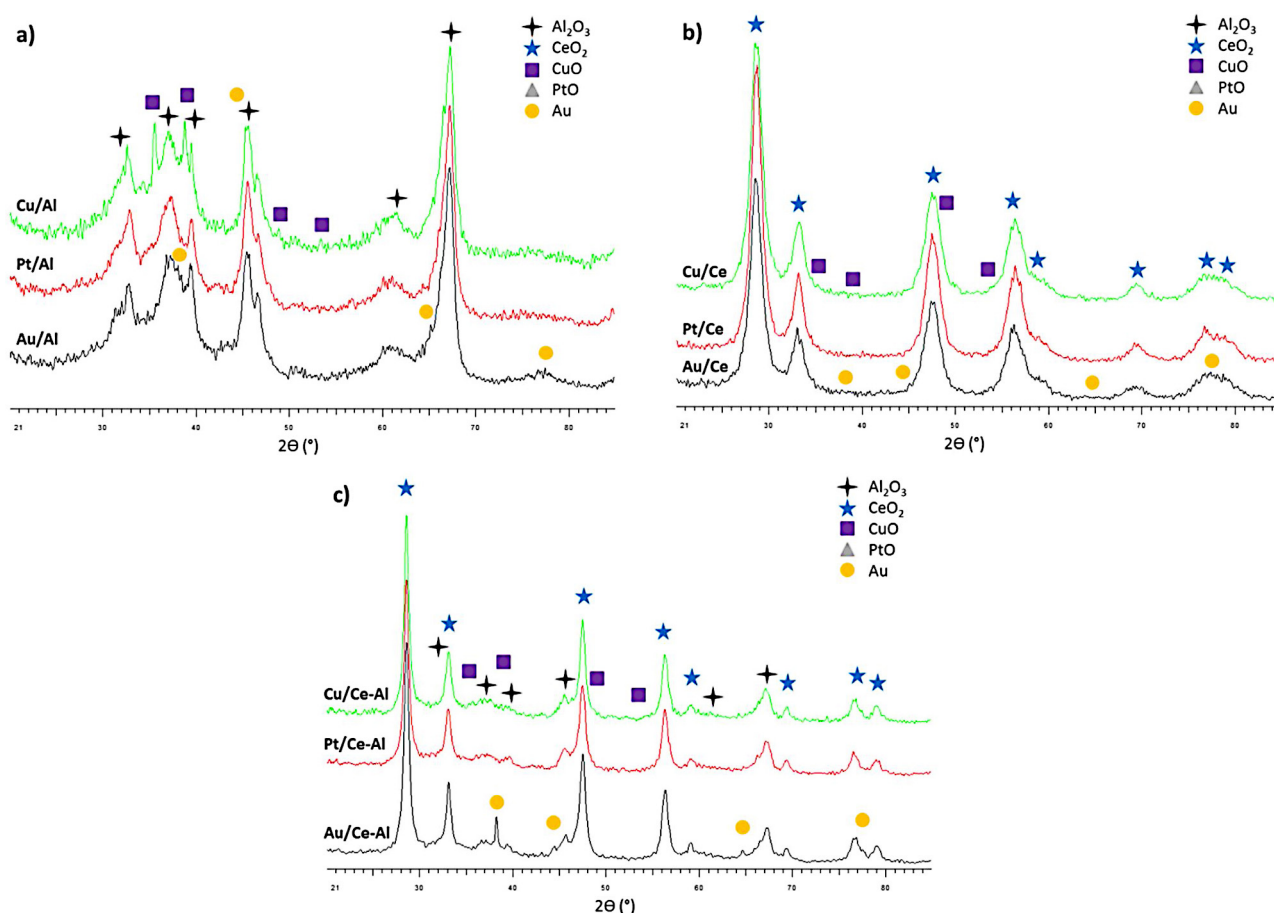


Fig. 2. XRD patterns of (a) Au, Pt, and Cu supported on  $\gamma$ - $\text{Al}_2\text{O}_3$ , (b) Au, Pt, and Cu supported on  $\text{CeO}_2$ , and (c) Au, Pt, and Cu supported on  $\text{CeO}_2$ - $\text{Al}_2\text{O}_3$ .

supported catalysts in Fig. 2a confirm the presence of alumina, copper oxide, and gold. The  $\text{Al}_2\text{O}_3$  support showed characteristic peaks according to JCPDS 088-0107,  $\text{CuO}$  according to JCPDS 048-1548, and Au according to JCPDS 071-3755, attributed to large crystallite sizes. However, the diffraction patterns of Pt species in the form of PtO or Pt are not observed, which could be due to high dispersion and small size of the Pt particles as a result of good impregnation and calcination at  $600^\circ\text{C}$ . According to Moroz et al. [40], since the most intense  $\text{Au}(111)$ ,  $\text{Au}(200)$ , and  $\text{Au}(220)$  peaks are superposed with the peaks from the  $\text{Al}_2\text{O}_3$  phase, the  $\text{Au}(311)$  peak, at  $2\theta = 77.5^\circ$ , can be used for the crystallite size determination. However, in the case of Au catalyst prepared by deposition-precipitation, the  $\text{Au}(311)$  peak is usually strongly broadened as shown in Fig. 2a and thus its width could not be measured accurately.

In case of  $\text{CeO}_2$  supported catalysts (Fig. 2b) the diffraction patterns confirm the presence of ceria in accordance to JCPDS 043-1002. Copper oxide and gold are not seen clearly. Cu could be in amorphous state not giving clear peaks in the pattern. The anticipated peaks of Au are superposed with ceria and CuO and/or the particle size of Au is too small in order to cause intense diffraction peaks. Platinum species are not observed in the form of PtO or Pt as in case of alumina.

Considering  $\text{CeO}_2$ - $\text{Al}_2\text{O}_3$  supported catalysts in Fig. 2c the diffraction patterns reveal clearly the presence of ceria, alumina, and Au. The  $\text{CeO}_2$ - $\text{Al}_2\text{O}_3$  support showed characteristic peaks of alumina according to JCPDS 088-0107, ceria according to JCPDS 043-1002, and Au according to JCPDS 065-2870. Copper oxide is not seen clearly most likely due to the amorphous state. Platinum species could not be detected as in the case of alumina and

ceria supported catalysts. Au peaks were clearly visible indicating a larger crystallite size which most likely originates from the high chlorine content observed by XRF. Ivanova et al. [41] showed that chlorine induces sintering during calcination, which further results in larger particle size of Au.

$\text{H}_2$ -TPR was used to determine the reducibility of the prepared catalysts. Fig. 3a–d shows the hydrogen uptakes of calcined Au, Pt, and Cu catalysts on different supports. Table 3 shows the theoretical and measured hydrogen consumptions in the experiments. The theoretical values were calculated for different oxidation states of the metal. The effect of support was deduced from the  $\text{H}_2$  uptakes.

The supports were also tested in  $\text{H}_2$ -TPR experiments (Fig. 3a). In the range of  $35$ – $400^\circ\text{C}$  no  $\text{H}_2$  uptake was detected in the case of  $\gamma$ - $\text{Al}_2\text{O}_3$  support as expected. Moreover,  $\text{CeO}_2$  and  $\text{CeO}_2$ - $\text{Al}_2\text{O}_3$  supports showed a  $\text{H}_2$  consumption starting from around  $350^\circ\text{C}$ . These findings are in accordance with the previous studies on  $\text{CeO}_2$  based catalysts [42–45]. In the supports containing several metal oxides with cerium oxide  $\text{H}_2$  uptake is mainly due to the reduction of cerium oxide. The  $\text{H}_2$  consumption values presented in Table 3 show that the measured  $\text{H}_2$  consumption is always somewhat higher than expected based on the theoretical  $\text{H}_2$  consumption of oxide form of Au, Pt or Cu. This indicates that also the support is reduced (especially when cerium oxide is concerned) or the catalyst contains certain impurities such as oxychlorides that are reduced during the  $\text{H}_2$ -TPR experiment.

The  $\text{H}_2$ -TPR profiles of Au-containing catalysts are shown in Fig. 3b. One can observe that in the case of  $\gamma$ - $\text{Al}_2\text{O}_3$  and  $\text{CeO}_2$ - $\text{Al}_2\text{O}_3$  supported catalysts no significant hydrogen uptake was recorded. Considering the Au/Ce catalyst, a large peak is observed between  $100$  and  $200^\circ\text{C}$ , with a maximum consumption between  $106$  and

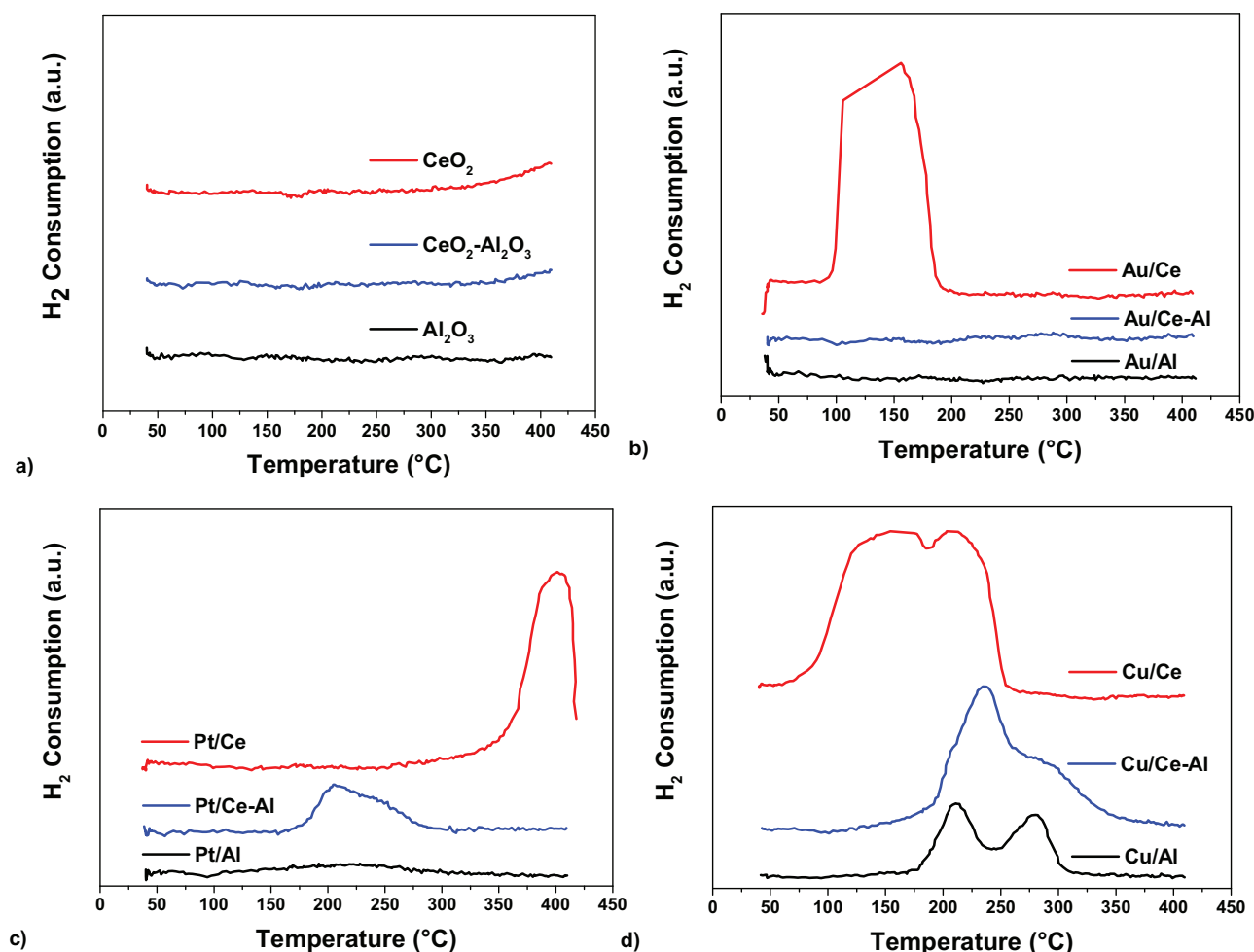


**Fig. 3.** H<sub>2</sub>-TPR profiles of (a)  $\gamma$ -Al<sub>2</sub>O<sub>3</sub>, CeO<sub>2</sub>, and CeO<sub>2</sub>-Al<sub>2</sub>O<sub>3</sub> supports (b) Au on  $\gamma$ -Al<sub>2</sub>O<sub>3</sub>, CeO<sub>2</sub>, and CeO<sub>2</sub>-Al<sub>2</sub>O<sub>3</sub> supports, (c) Pt on  $\gamma$ -Al<sub>2</sub>O<sub>3</sub>, CeO<sub>2</sub>, and CeO<sub>2</sub>-Al<sub>2</sub>O<sub>3</sub> supports, as well as (d) Cu on  $\gamma$ -Al<sub>2</sub>O<sub>3</sub>, CeO<sub>2</sub>, and CeO<sub>2</sub>-Al<sub>2</sub>O<sub>3</sub> supports.

**Table 3**

Hydrogen consumptions in the H<sub>2</sub>-TPR experiments.

Catalyst	Theoretical H <sub>2</sub> consumption (μmol g <sup>-1</sup> )			Measured H <sub>2</sub> consumption (μmol g <sup>-1</sup> )
	Oxidation state			
	1+	2+	3+	
Au/Al	18	36	54	52
Pt/Al	28	56	–	149
Cu/Al	401	803	–	1461
Au/Ce	24	47	71	–
Pt/Ce	29	57	–	903
Cu/Ce	441	881	–	3119
Au/Ce-Al	12	23	35	83
Pt/Ce-Al	31	62	–	326
Cu/Ce-Al	456	913	–	1690

156 °C, which is in line with the previous studies [43–45,46–49]. Fu et al. [46] found out that the surface oxygen of ceria is substantially weakened by the presence of Au nanoparticles, its reduction temperature shifting by several hundred degrees to 100 °C or lower. Andreeva et al. [49] suggested that the low-temperature peak appearing for CeO<sub>2</sub> at around 500 °C is assigned to the reduction of surface oxygen species. According to Liu et al. [45] the deposition of Au shifted the reduction peak of CeO<sub>2</sub> to around 110 °C and referred that highly dispersed Au can dissociate H<sub>2</sub> below 150 °C, which enhances the reduction of CeO<sub>2</sub> due to a hydrogen spillover. Scirè et al. [42] observed a peak at 140 °C and referred that the presence of Au promotes the reduction of surface oxygen species due

to the weakening of the surface Ce–O bond caused by the presence of Au. Solsona et al. [44] found a peak maximum at 117 °C and suggested that the enhancement is probably a consequence of defects on the surface of the support due to the creation of new sites at the boundary of the Au particles and the oxide surface.

The size of Au particle affects the reducibility. It is known that only very small particles of Au can dissociate hydrogen at low temperatures. In our case the size of Au particles in Au/Ce-Al were much larger than in case of Au/Al or Au/Ce catalysts evidenced by XRD and HR-TEM. Fig. 4a and b shows the HR-TEM images of Au/Al catalyst. The surface of the sample in Fig. 4a was analyzed with EDS which showed the presence of homogeneously dispersed Au

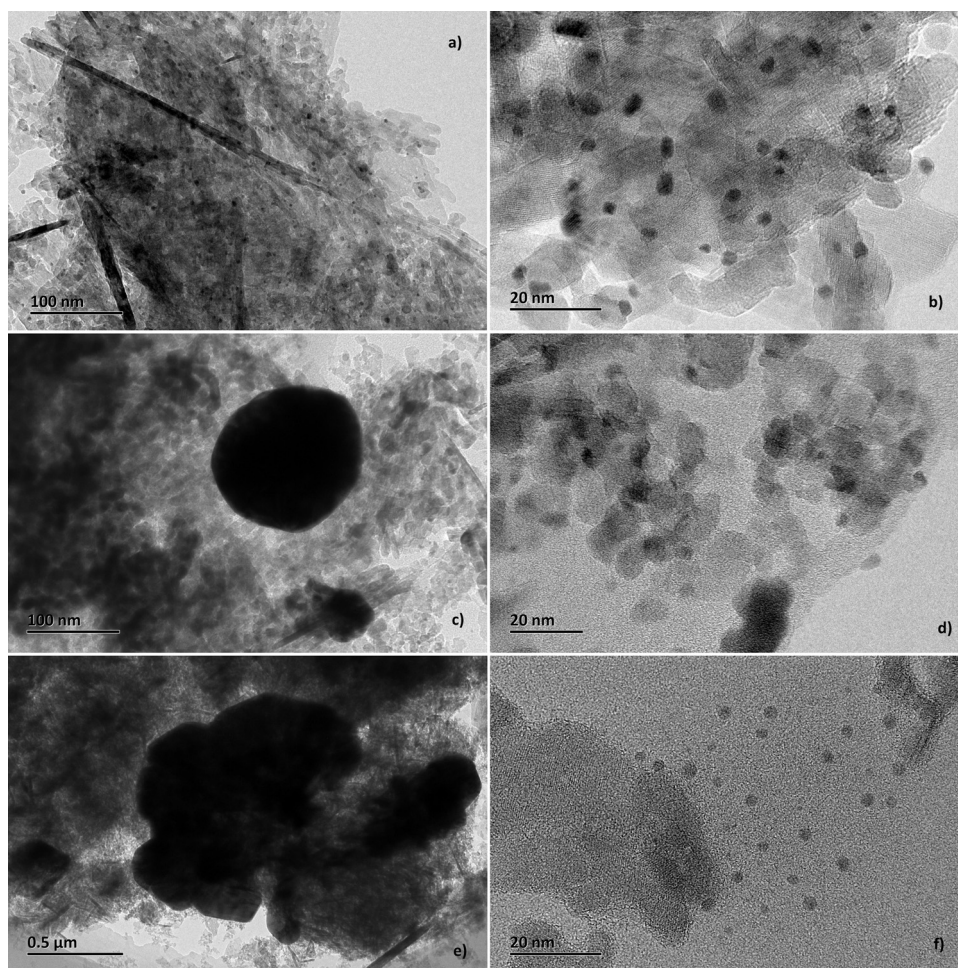


**Fig. 4.** HR-TEM images of Au/Al catalyst (a and b), Au/Ce-Al catalyst (c and d) and Cu/Al catalyst (e and f).

in size smaller than 10 nm. In contrary, the Au/Ce-Al catalyst presented in Fig. 4c and d displayed large Au clusters confirmed by EDS with sizes of 100–200 nm. Interestingly, Au/Ce-Al catalyst did not show any major consumption of hydrogen during the TPR experiment. It seems that the particle size of Au was not small enough to induce hydrogen dissociation on the catalyst surface, and thus no  $H_2$  uptake was seen during the TPR experiment.

The  $H_2$ -TPR profiles of Pt-containing catalysts are shown in Fig. 3c. In the case of Pt/Al catalyst, a minor  $H_2$  uptake was observed within a broad temperature range of around 100 to 300 °C with a peak maximum at 229 °C. In addition, a very minor uptake of  $H_2$  was seen within the temperature range of 50–70 °C that could have been originating from the reduction of adsorbed oxygen species. Abbasi et al. [50] observed a small reduction peak for (1%)Pt/ $Al_2O_3$  in the temperature range of about 260–500 °C, with a maximum at 290 °C attributed to the reduction of Pt-oxide species and/or of  $PtCl_xO_y$  (platinum oxychlorides surface complexes) species. Pitkääho et al. [51] noticed peaks centered at 70 °C and 230 °C in the  $H_2$ -TPR profile of catalyst containing 1 wt.% of Pt on  $Al_2O_3$ , which could be attributed to the reduction of adsorbed oxygen on alumina and the reduction of Pt-oxides, respectively. The addition of Pt enhances the reduction of ceria as seen in the case of Pt/Ce where the peak maximum was shifted to 400 °C compared with the pure ceria support that had the strongest peak at temperatures higher than 410 °C. Pt also improved the reduction of the  $CeO_2$ - $Al_2O_3$  support as expected. A peak maximum was observed at 205 °C. In addition, a shoulder was observed which could be explained by the reduction of Pt species and by the fact that the presence of Pt on

$CeO_2$  surface facilitates the reduction of the surface  $CeO_2$  due to the hydrogen spillover as suggested by Abbasi et al. [50]. They found a peak centered at around 270 °C with a shoulder at 340 °C in the case of the (1%)Pt/ $Al_2O_3$ - $CeO_2$ (30%) catalyst, which were attributed to the reduction of platinum oxychlorides complexes as well to the reduction of superficial ceria promoted by Pt.

The  $H_2$ -TPR profiles of Cu-containing catalysts are displayed in Fig. 3d. Due to the calcination at 600 °C copper oxides are likely to be present. Clear reduction peaks, centered at 211 °C and 280 °C, were observed for the Cu/Al catalyst. Similar types of observations were done in the case of Cu/Ce and Cu/Ce-Al catalysts. Cu/Ce showed reduction peaks at lower temperatures, centered at 154 °C and 203 °C. For the Cu/Ce-Al catalyst, a peak maximum was found at 234 °C overlapped with a shoulder at higher temperatures. Comparable results were observed for alumina supported Cu catalyst by Wang and Weng [11], who found double peaks at around 260–280 °C and 210–230 °C, and referred that the high temperature peak represents the crystal phase of copper oxide and the low temperature peak might be attributed to the amorphous phase of copper oxide. Matching peaks were observed by Dow et al. [52] when copper oxide is supported on  $\gamma$ - $Al_2O_3$ . The peak maximum at around 210 °C is attributed to the reduction of highly dispersed copper oxide species, which cannot be detected by XRD. The peak at higher temperature of around 245 °C is ascribed to the reduction of large three-dimensional clusters and bulk CuO phase that have characters and properties identical to those of pure CuO powder, which can be detected by XRD. In our case we also observed different sizes of copper oxide particles based on HR-TEM (Fig. 4e and f).

Dow et al. observed also that the amounts of the highly dispersed copper oxide species can be increased and the amounts of the bulk-like CuO can be decreased by the reoxidation treatment due to the occurrence of redispersion [52]. Similarities were observed for the ceria supported Cu catalyst. Zhang et al. [53] detected a two-step reduction profile for the CuO/CeO<sub>2</sub> catalyst prepared via conventional impregnation. The peak maxima were found around 150 °C and 190 °C, which revealed that CeO<sub>2</sub> enhances the reduction of CuO species, and the smaller the CuO particles, the easier the reduction. Kundakovic and Flytzani-Stephanopoulos [54] studied the reduction characteristics of Cu (5%) loaded on La doped ceria and showed that the reduction by H<sub>2</sub> gives a broad peak with a maximum at around 175 °C. Copper is present as highly dispersed clusters or as isolated Cu ions. They found a clear influence of the host oxide on the reduction behavior of copper. In turn, copper enhances the reducibility of ceria [54].

The TPIE experiments with labeled oxygen were carried out for all the catalysts and their corresponding supports. The evolutions of the rate of oxygen exchange ( $R_e$ ) and the number of exchanged oxygen atoms ( $N_e$ ) are shown in Figs. 5 and 6a–c, respectively, both with respect to temperature, and in Table 4. The catalysts are able to exchange oxygen in a specific temperature range depending on the support and the added metal phase.

The catalysts supported on Al<sub>2</sub>O<sub>3</sub> and CeO<sub>2</sub>-Al<sub>2</sub>O<sub>3</sub> activate oxygen in broader temperature ranges compared to the CeO<sub>2</sub> supported catalysts. It is known that the <sup>16</sup>O<sub>2</sub>/<sup>18</sup>O<sub>2</sub> isotopic equilibration on metals is a structure and support-sensitive reaction, particularly with reducible supports which can lead to the SMSI effects [55]. In addition, chlorine ions have a hindering effect on the equilibration reaction. Typically Cl ions are located on the support in the vicinity of the metal particles. Furthermore, it has been observed that part of the Cl atoms is still bound to the metal particles after high-temperature oxidation or reduction, which can elucidate the inhibiting role of chlorine in equilibration [55]. The precursor salts used for the preparation of the CeO<sub>2</sub>-Al<sub>2</sub>O<sub>3</sub> support, wet impregnation of Pt, and deposition of Au contained chlorine that may have an effect on the oxygen activation in our case as well.

On bare alumina the formation of <sup>18</sup>O<sup>16</sup>O was detected to begin at around 440 °C. The order of the lowest starting temperatures, in the case of alumina catalysts, were Cu/Al < Au/Al = Pt/Al < Al, respectively (Fig. 5a). The Cu/Al catalyst showed the formation of <sup>18</sup>O<sup>16</sup>O at around 360 °C. The addition of a metal phase lowered the initial temperature of the accelerated exchange rate substantially as expected in the case of alumina supported catalysts. The addition of metal phase did not increase extensively the amounts of exchanged oxygen atoms in the case of alumina supported catalysts.

In the case of bare ceria support, the formation of <sup>18</sup>O<sup>16</sup>O (0.1 mbar at around 230 °C) was observed in the beginning of the experiment. Among the ceria based catalysts, the order of the lowest starting temperatures were Au/Ce < Cu/Ce < CeO<sub>2</sub> < Pt/Ce (Fig. 5b). The formation of <sup>18</sup>O<sup>16</sup>O was observed with Au/Ce (1 mbar at around 270 °C) in the beginning of the experiment similarly to the ceria support. In the case of Pt/Ce and Cu/Ce, the formation of <sup>18</sup>O<sup>16</sup>O was seen to start at around 330 °C and 300 °C, respectively. The added metal phase facilitated the activation of oxygen similarly as in the case of alumina support, since increasing exchange rates were seen at lower temperature ranges compared to the alumina based catalysts. The bare ceria supported catalysts seem to activate surface oxygen already at lower temperatures compared to the rest of the used supports. Compared to the Au, Pt, and Cu doped samples the bare ceria exhibits the highest exchange rates, but the lowest number of exchanged oxygen atoms, which could be explained by the preparation method with the added metal phase. The precursor salts used for the wet impregnation of Pt and deposition of Au, con-

tained chlorine that may have an effect on the oxygen activation as mentioned earlier.

The CeO<sub>2</sub>-Al<sub>2</sub>O<sub>3</sub> support, Au/Ce-Al, and Pt/Ce-Al showed similar performances (Fig. 5c). Interestingly, only the addition of Cu facilitated the activation of oxygen by lowering the temperature level, where exchange rate started to increase considerably, among CeO<sub>2</sub>-Al<sub>2</sub>O<sub>3</sub> supported catalysts.

### 3.2. Catalytic tests

#### 3.2.1. Oxidation of CH<sub>3</sub>SSCH<sub>3</sub>

The CH<sub>3</sub>SSCH<sub>3</sub> light-off curves for all the prepared catalysts and corresponding supports are displayed in Fig. 7a–c.

Complete CH<sub>3</sub>SSCH<sub>3</sub> conversion was reached in the temperature range from 300 °C to 600 °C over most of the catalysts (Fig. 7a–c). The  $T_{25}$ ,  $T_{50}$ ,  $T_{90}$ , and  $T_{100}$  temperature values of oxidized CH<sub>3</sub>SSCH<sub>3</sub> are shown in Table 5. The specific surface areas ( $S_{BET}$ ) did not affect the CH<sub>3</sub>SSCH<sub>3</sub> conversion, or SO<sub>2</sub> and CH<sub>2</sub>O formations substantially. In terms of the  $T_{50}$  values (that represent the light-off point of the catalysts), the Cu/Ce-Al catalyst showed the best activity in CH<sub>3</sub>SSCH<sub>3</sub> oxidation (Fig. 7c) followed by Cu/Al (Fig. 7a) and Cu/Ce (Fig. 7b). With the Cu/Ce-Al catalyst CH<sub>3</sub>SSCH<sub>3</sub> oxidation started at around 250 °C and full conversion was reached at 325 °C (Fig. 7c). The next best catalysts reaching 100% conversion were Cu/Al (Fig. 7a) and Pt/Al (Fig. 7a), at substantially higher temperatures, i.e., at around 545 °C and 550 °C, respectively. Noteworthy, Cu containing catalysts showed higher activity when compared to the Pt and Au containing catalysts. Au did not provide significant improvement in the oxidation of CH<sub>3</sub>SSCH<sub>3</sub>, especially when higher conversions were considered as was expected based on refs. [25,28]. The rather low activity could be explained by the sintering of small Au particles in the high temperature calcination at 600 °C due to the relatively low melting point of <10 nm Au particles (below ~530 °C), resulting in less active catalysts [56]. The preparation method of deposition-precipitation with urea used in this study is known to form Au particles in the size range of 1–6 nm [36]. When Au and Pt catalysts were compared, Au catalysts oxidized CH<sub>3</sub>SSCH<sub>3</sub> better at low and intermediate temperatures, as anticipated [28]. Interestingly, CeO<sub>2</sub>-supported catalysts started adsorbing CH<sub>3</sub>SSCH<sub>3</sub> already at around 140 °C. Au/Ce began to adsorb at 140 °C and the oxidation to SO<sub>2</sub> was observed at 190 °C. Similarly, Pt/Ce started to adsorb CH<sub>3</sub>SSCH<sub>3</sub> at around 140 °C and the formation of SO<sub>2</sub> was detected at 180 °C. In the case of Cu/Ce, the consumption of CH<sub>3</sub>SSCH<sub>3</sub> was seen to start at around 170 °C at the same temperature as the formation of SO<sub>2</sub>. Moreover, the light-off curves over CeO<sub>2</sub>-supported catalysts were in broader temperature ranges. The CeO<sub>2</sub> support by itself, i.e., without any additional metal on the surface, showed considerable activity.

#### 3.2.2. Yields of various products

The total oxidation of CH<sub>3</sub>SSCH<sub>3</sub> is desired in order to have SO<sub>2</sub>, CO<sub>2</sub> and water as the final products of oxidation. The SO<sub>2</sub> yields for all the prepared catalysts and corresponding supports are shown in Fig. 8a–c. In this study over 100% yields for SO<sub>2</sub> and CO<sub>2</sub> were observed most probably due to adsorption-desorption phenomenon. Adsorption of CH<sub>3</sub>SSCH<sub>3</sub> was seen at temperatures lower than 100 °C and therefore desorption and reaction at higher temperatures resulting yields higher than 100% were possible. This was more noticeable in case of alumina containing catalysts. It is known that in oxidizing conditions, at around 400 °C sulfur can be stored in the material through the oxidation of SO<sub>2</sub> to form SO<sub>3</sub> that reacts with alumina to form sulfates [57]. This sulfur could be released at higher temperatures. According to Waqif et al. [58], the oxidative adsorption of SO<sub>2</sub> on ceria leads to the formation of two types of sulfate species on the surface: bulk and surface species, the latter being formed more easily. Bulk species which were formed by

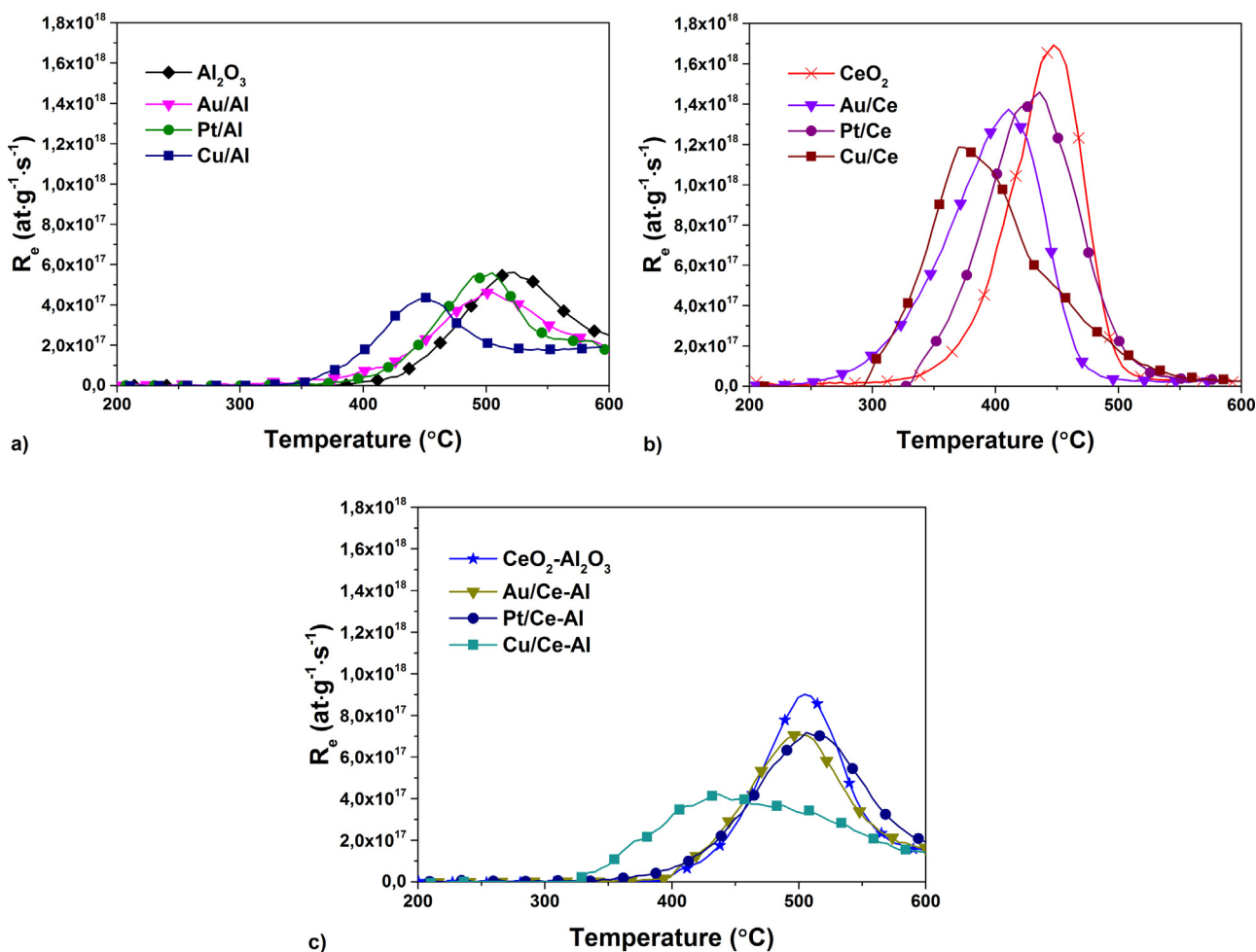


**Fig. 5.** Evolution of the rate of oxygen exchange in the TPIE experiments with labeled oxygen (<sup>18</sup>O<sub>2</sub>) for (a) Au, Pt, and Cu on  $\gamma$ -Al<sub>2</sub>O<sub>3</sub>, (b) Au, Pt, and Cu on CeO<sub>2</sub>, as well as (c) Au, Pt, and Cu on CeO<sub>2</sub>-Al<sub>2</sub>O<sub>3</sub> catalysts ( $R_e$  = rate of oxygen exchange).

**Table 4**

Results of the TPIE experiments for all the prepared catalysts and corresponding supports.

Catalyst	Temperature range of exchange (°C)	Temperature of max. rate (°C)	$R_e$ max. (10 <sup>17</sup> at g <sup>-1</sup> s <sup>-1</sup> )	$N_e$ final at 600 °C (10 <sup>21</sup> at g <sup>-1</sup> )
Au/Al	310→	500	4.61	1.83
Pt/Al	370→	500	5.59	1.80
Cu/Al	340→	450	4.36	1.68
Au/Ce	230–510	410	13.7	4.24
Pt/Ce	330–550	440	14.6	4.30
Cu/Ce	290–560	370	11.9	4.00
Au/Ce-Al	380→	500	7.08	2.24
Pt/Ce-Al	340→	510	7.18	2.45
Cu/Ce-Al	320→	440	4.21	2.18
Support				
Al <sub>2</sub> O <sub>3</sub>	390→	520	5.60	1.86
CeO <sub>2</sub>	310–540	450	16.9	3.90
CeO <sub>2</sub> -Al <sub>2</sub> O <sub>3</sub>	370→	510	9.03	2.44

$R_e$  = rate of oxygen exchange.

$N_e$  = number of exchanged oxygen atoms.

oxidation of SO<sub>2</sub> under excess of oxygen at 400 °C are not very stable because a major part of the bulk species formed had disappeared at 600 °C. SO<sub>2</sub> species remained adsorbed at 400 °C and they are then oxidized by O<sub>2</sub>. Another study by Waqif et al. [59] done with CeO<sub>2</sub>-Al<sub>2</sub>O<sub>3</sub> using thermogravimetric experiments revealed that the sulfate species adsorbed on CeO<sub>2</sub> at lower temperatures start to decompose at above 400 °C. They concluded that ceria enhances the oxidation of SO<sub>2</sub> into sulfates, which are thermally more stable on

CeO<sub>2</sub>-Al<sub>2</sub>O<sub>3</sub> than on ceria, but less stable and more easily reducible by H<sub>2</sub> compared sulfates on alumina. In addition, it is known that sulfation of ceria results in a loss of surface area and the blocking of the small mesopores – thus, affecting the activity. This is probably a consequence of measured crystallite size growth due to sintering [60]. According to Kylhammar et al. [61] sulfur oxides are stored at temperatures between 200 and 500 °C and released slightly above 500 °C under lean conditions. Alumina and ceria do not release any

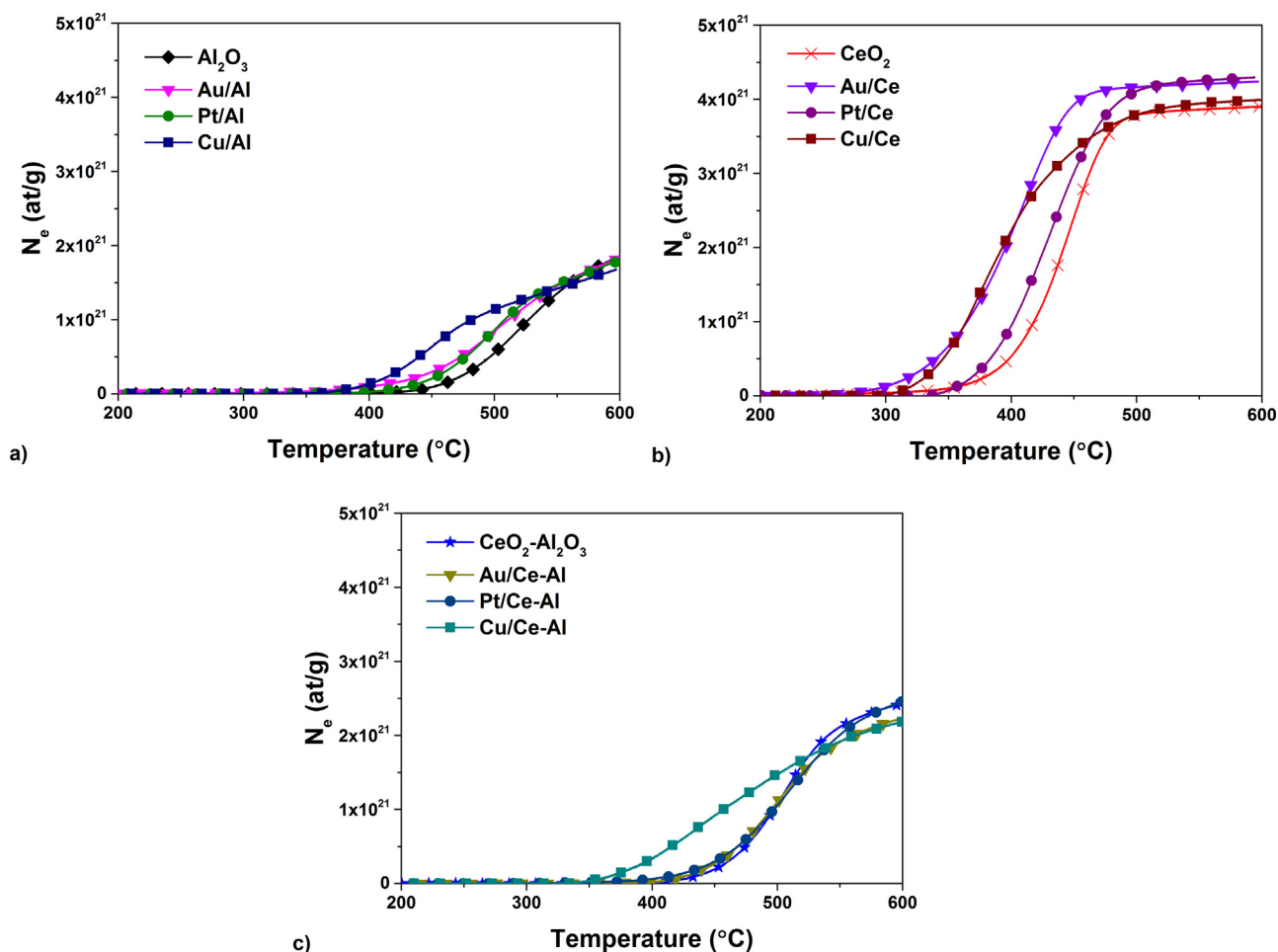


**Fig. 6.** Evolution of the number of exchanged oxygen atoms in the TPIE experiments with labeled oxygen  $^{18}\text{O}_2/^{16}\text{O}_2$  for (a) Au, Pt, and Cu on  $\gamma\text{-Al}_2\text{O}_3$ , (b) Au, Pt, and Cu on  $\text{CeO}_2$ , as well as (c) Au, Pt, and Cu on  $\text{CeO}_2\text{-Al}_2\text{O}_3$  catalysts ( $N_e$  = number of exchanged oxygen atoms).

**Table 5**

The  $T_{25}$ ,  $T_{50}$ ,  $T_{90}$ , and  $T_{100}$  temperatures of oxidized  $\text{CH}_3\text{SSCH}_3$  for all the prepared catalysts and their corresponding supports, ( $\pm 5^\circ\text{C}$ ). The best values are indicated.

Catalyst	$T_{25}$	$T_{50}$	$T_{90}$	$T_{100}$
Au/Al	320	350	420	600
Pt/Al	370	390	415	550
Cu/Al	<u>230</u>	280	400	545
Au/Ce	290	350	480	580
Pt/Ce	255	325	435	*
Cu/Ce	260	300	445	*
Au/Ce-Al	280	405	525	*
Pt/Ce-Al	290	380	460	*
Cu/Ce-Al	270	<u>275</u>	<u>290</u>	<u>325</u>
Support				
$\text{Al}_2\text{O}_3$	395	420	505	*
$\text{CeO}_2$	235	360	480	*
$\text{CeO}_2\text{-Al}_2\text{O}_3$	340	375	440	*

\*Not reached up to  $600^\circ\text{C}$ .

significant amounts of sulfur oxides below  $500^\circ\text{C}$ . The addition of Pt on ceria enhances the  $\text{SO}_x$  storage capacity by increasing the rate of bulk sulfate formation. The  $\text{SO}_x$  desorption begins at around  $500^\circ\text{C}$  indicating that thermal decomposition of  $\text{SO}_x$  adsorbed on ceria is important [62]. These findings support the assumption that the formed sulfate species are desorbed at temperatures higher than  $400^\circ\text{C}$  resulting in  $\text{SO}_2$  yields over 100%.

Although the  $\text{SO}_2$  yields over the sample catalysts were at similar level (Fig. 8a–c), the addition of noble metal decreased the formation of formaldehyde ( $\text{CH}_2\text{O}$ ) and carbon monoxide (CO) as

un-wanted reaction products. The  $\text{CH}_2\text{O}$  yields and CO concentrations during  $\text{CH}_3\text{SSCH}_3$  oxidation are shown in Figs. 9 and 10a–c, respectively. In general, the lowest amounts of un-wanted products were formed over Pt containing catalysts (Figs. 9 and 10a–c). Results unfortunately support the assumption that  $\text{SO}_2$  is further oxidized over Pt catalysts, which is more visible in case of alumina supported catalyst. The rapid loss in  $\text{SO}_2$  production was not observed in case of Pt/Ce catalyst, which is promising.

In the case of Cu-containing catalysts the formation of  $\text{CH}_2\text{O}$  was substantial and independent on the support used (Fig. 9a–c).  $\text{CH}_2\text{O}$

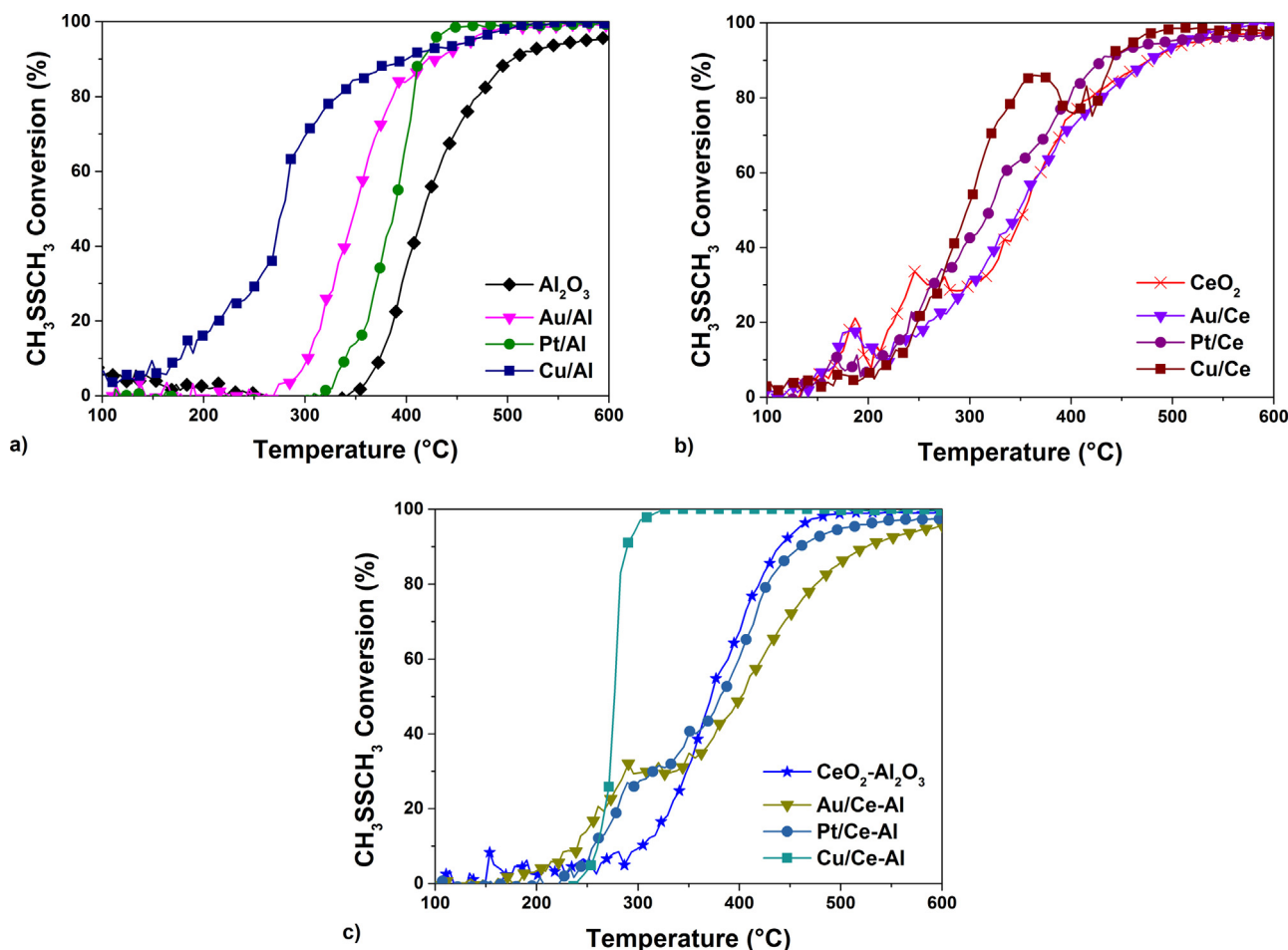


Fig. 7. The light-off curves of (a) Au, Pt, and Cu on  $\gamma\text{-Al}_2\text{O}_3$ , (b) Au, Pt, and Cu on  $\text{CeO}_2$ , as well as (c) Au, Pt, and Cu on  $\text{CeO}_2\text{-Al}_2\text{O}_3$  catalysts in the oxidation of  $\text{CH}_3\text{SSCH}_3$ .

formation seems to be promoted by copper itself. The addition of ceria in case of Au and Pt catalysts increases the  $\text{CH}_2\text{O}$  production. Thus, ceria seems to enhance the  $\text{CH}_2\text{O}$  formation as well. Pt/Ce catalyst showed a rapid decrease and a subsequent increase in  $\text{CH}_2\text{O}$  formation in the temperature range of about 400–500  $^{\circ}\text{C}$ , which were connected to a comparable decrease in CO formation and increase in  $\text{CO}_2$  formation. Both Pt/Ce and Cu/Ce catalysts showed double peaks in  $\text{CH}_2\text{O}$  concentrations, which was not seen in case of Au/Ce catalyst.

The  $\text{CeO}_2$  containing catalysts were noticed to be  $\text{SO}_2$  selective at higher temperatures and could hold the key to avoid sulfuric acid formation. The Au/Ce-Al catalyst and  $\text{CeO}_2$  support solely seem promising in terms of selectivity, since both give good selectivities towards  $\text{SO}_2$  as seen in Fig. 8b and c. The addition of Au also promoted  $\text{CO}_2$  formation at higher temperatures. Moreover,  $\text{CH}_2\text{O}$  was formed at the temperatures of 400  $^{\circ}\text{C}$  to 500  $^{\circ}\text{C}$  without excessive CO formation (Fig. 10c). The Au/Ce-Al is particularly of interest due to the assumed sulfur resistance of gold.  $\text{CeO}_2$  showed major decrease in activity, but the Au/Ce-Al catalyst performed better giving only a minor decline in  $\text{CH}_3\text{SSCH}_3$  conversion when the repeated light-off tests were considered as well. However, it is important to notice that when designing a catalyst for total oxidation of SVOCs, the formation of  $\text{CH}_2\text{O}$  is not a beneficent property and finally should be avoided.

When taking into account all un-wanted reaction products the most appropriate catalyst was Cu/Al. It should be operated well above  $T_{100}$ , even over 600  $^{\circ}\text{C}$ , to avoid the formation of  $\text{CH}_2\text{O}$  and CO. The problem is that the production of  $\text{SO}_2$  is also decreased. If we can accept a slight formation of  $\text{CH}_2\text{O}$  and CO the optimal tem-

perature range of operation is 500–550  $^{\circ}\text{C}$ . However, Pt/Al catalyst would also allow to avoid the formation of undesired products, but in a really narrow temperature window at 425  $^{\circ}\text{C}$ . The Pt/Ce catalyst is a good option in the temperature range of 400–500  $^{\circ}\text{C}$ . However, 100% conversion of  $\text{CH}_3\text{SSCH}_3$  was not achieved. Thus, the solution could be a bimetallic catalyst, which would be also important in improving the stability of Cu/Al [11] and Pt/Al [5].

In general, Au did not improve significantly the yields over the supports in the oxidation of  $\text{CH}_3\text{SSCH}_3$ —only the formation of  $\text{CO}_2$  was higher at lower temperatures. The best yields towards  $\text{CO}_2$  were achieved over Pt containing catalysts, that gave yields ranging from approximately 50 to 100% in the temperature range from roughly 400 to 600  $^{\circ}\text{C}$ . In case of Pt/Ce catalyst, high yields of both,  $\text{CO}_2$  and  $\text{SO}_2$ , were reached in the temperature window of around 400–480  $^{\circ}\text{C}$  after which the  $\text{CO}_2$  yield dropped drastically. Over the Cu containing catalysts the  $\text{CO}_2$  yield was very low due to the considerably high formation of the partial oxidation product,  $\text{CH}_2\text{O}$ , at low and moderate temperatures. Cu/Al and Cu/Ce-Al both reached over 80%  $\text{CO}_2$  yields at higher temperature level of about 530  $^{\circ}\text{C}$ . However, Cu catalysts showed lower starting temperatures for the  $\text{CH}_3\text{SSCH}_3$  conversion. With noble metals the  $\text{CH}_3\text{SSCH}_3$  oxidation reaction starts at higher temperatures resulting in total oxidation products. Thus, the preparation of bimetallic catalysts combining all the benefits is worth of further investigation.

Considering the  $\text{H}_2$ -TPR experiments, it can be seen that the Cu containing catalysts consume more hydrogen than Au and Pt containing catalysts. It appears that Cu is in more oxidized state than Au and Pt, and therefore Cu oxides seem to provide more reactive oxygen to start the reaction with  $\text{CH}_3\text{SSCH}_3$  at lower temperatures

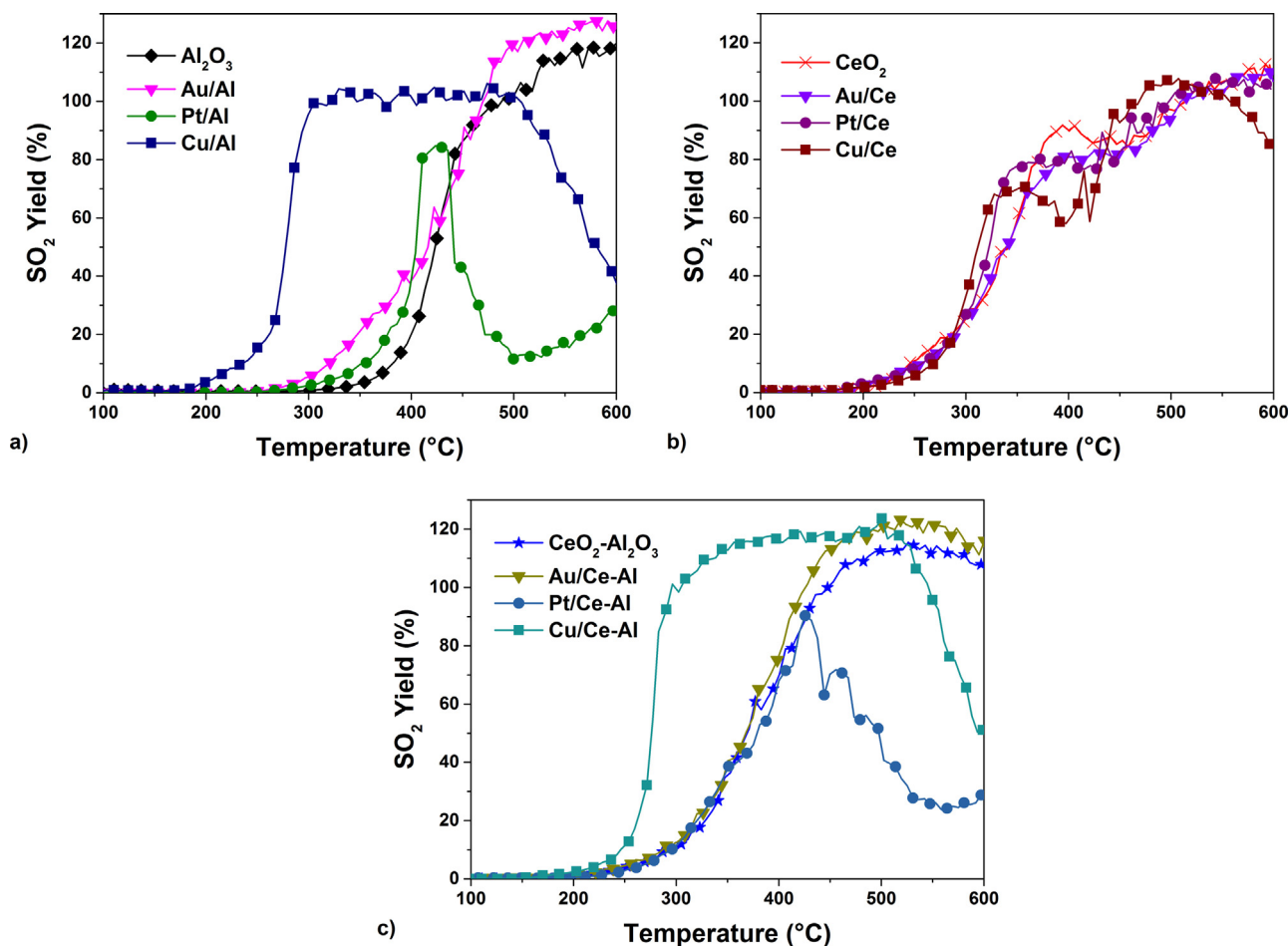


Fig. 8. The SO<sub>2</sub> yields over (a) Au, Pt, and Cu on  $\gamma$ -Al<sub>2</sub>O<sub>3</sub>, (b) Au, Pt, and Cu on CeO<sub>2</sub>, as well as (c) Au, Pt, and Cu on CeO<sub>2</sub>-Al<sub>2</sub>O<sub>3</sub> catalysts in the oxidation of CH<sub>3</sub>SSCH<sub>3</sub>.

compared to Au and Pt catalysts. In other words, here CuO and other quantitatively minor Cu oxides can release more oxygen from their structures for CH<sub>3</sub>SSCH<sub>3</sub> oxidation at lower temperatures, according to the Mars-van Krevelen mechanism, than Au and Pt can dissociate oxygen from the gas phase. These conclusions were supported by the isotopic exchange experiments discussed earlier. In a similar way, the addition of CeO<sub>2</sub> improved this desired property of the catalyst in all cases. However, in the case of Cu containing catalysts the reaction lead into partial oxidation of CH<sub>3</sub>SSCH<sub>3</sub>.

The formation of SO<sub>2</sub> seems to have a connection with the oxygen activation as well as the conversion of CH<sub>3</sub>SSCH<sub>3</sub>. The activation of oxygen started at lower temperatures in the case of Cu-containing catalysts compared to other metals with the corresponding supports, which seem to have an effect on the CH<sub>3</sub>SSCH<sub>3</sub> reaction resulting in lower conversion temperatures. Moreover, the effect was observed to be more significant in the case of alumina and CeO<sub>2</sub>-Al<sub>2</sub>O<sub>3</sub> supported catalysts. On the bare ceria support, differences between the catalysts were not substantial. Also the reducibility of the catalysts seemed to play a role with respect to oxidation products in the case of Cu catalysts, since the temperature areas matched quite well.

Interestingly, Scirè et al. [42] stated that Au prepared by deposition-precipitation on CeO<sub>2</sub> is more active than the one deposited by colloidal dispersion and there is a direct relationship between the surface oxygen mobility of the gold/oxide system and its catalytic activity. Observations support the fact that oxygen activation has connection to the formation of SO<sub>2</sub>. These findings were clearer in the case of Al and Ce-Al supported catalysts because Ce supported catalysts did not show significant differences. In this

study, the Au phase increased the activity significantly in the case of alumina supported catalysts, but did not reach the activity of Cu/Al. The conversion of CH<sub>3</sub>SSCH<sub>3</sub> started at a bit lower temperatures in the case of Au/Ce-Al catalyst (~170 °C), but no oxidation products at this temperature were formed, that could indicate the adsorption of CH<sub>3</sub>SSCH<sub>3</sub> on the surface, followed by possible splitting of the SS bond as mentioned in refs. [63–66].

### 3.2.3. Stability of Au/Ce-Al catalyst

According to the objectives of this study, the Au/Ce-Al catalyst was selected for a stability test (>40 h) at constant temperature of 475 °C, since CeO<sub>2</sub> containing catalysts showed good selectivity towards SO<sub>2</sub> formation at higher temperatures, especially in the case of Au loaded catalysts, which also showed better activity at lower temperatures compared to the Au/Al catalyst. Additionally, Au was assumed to enhance the stability. In the beginning of the stability test, the initial temperature was set based on the light-off test results of the Au/Ce-Al catalyst where T<sub>90</sub> was reached at 525 °C. However, in isothermal conditions at 525 °C, the conversion was around 98% and therefore the temperature was decreased during the first 30 min stepwise to correspond better to the expected 90% of conversion in order to see the deactivation better. The results of the long-term stability test (41.6 h) for the Au/Ce-Al catalyst are shown in Fig. 11a and b.

The conversion of CH<sub>3</sub>SSCH<sub>3</sub> remained stable during the whole testing period (Fig. 11a). During the first 30 min of the experiment the temperature of the oven was let to stabilize from 525 °C down to 475 °C, resulting in a minor decrease in the CH<sub>3</sub>SSCH<sub>3</sub> conversion. Throughout the stability test, a slight decline in the CH<sub>2</sub>O formation

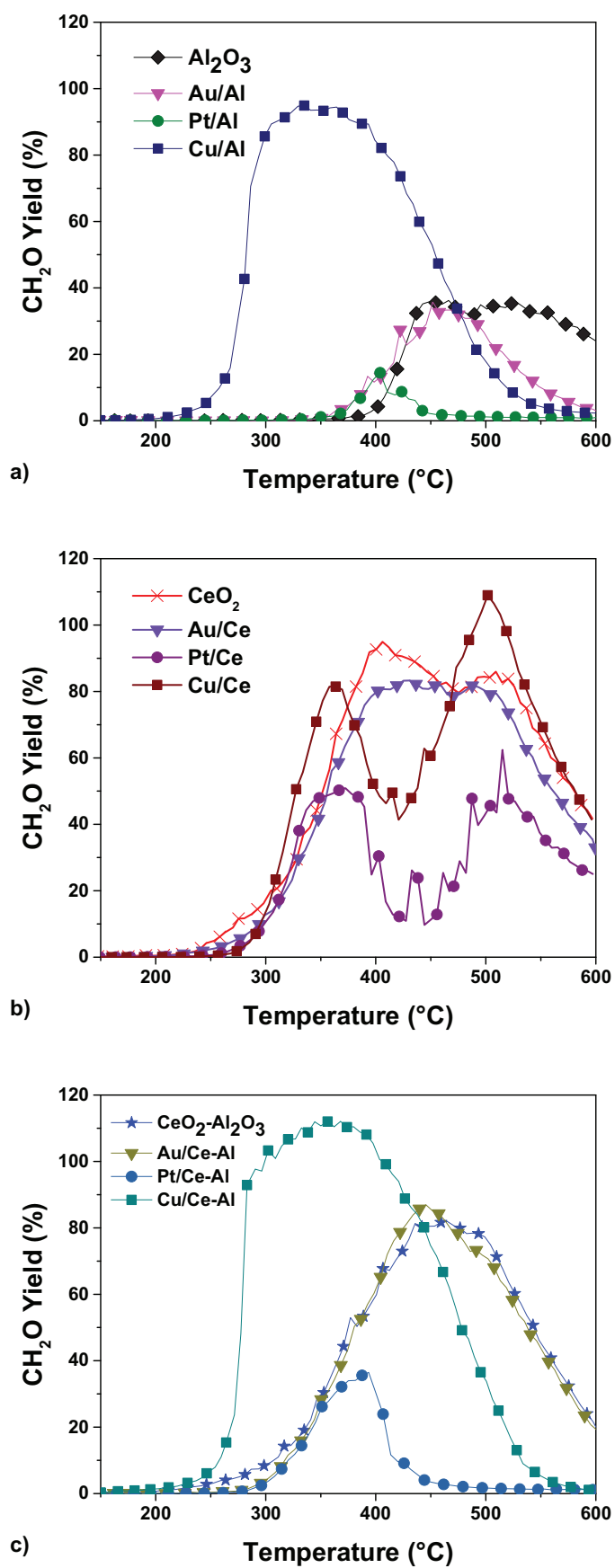


Fig. 9. CH<sub>2</sub>O yield over (a) Au, Pt, and Cu on  $\gamma$ -Al<sub>2</sub>O<sub>3</sub>, (b) Au, Pt, and Cu on CeO<sub>2</sub>, as well as (c) Au, Pt, and Cu on CeO<sub>2</sub>-Al<sub>2</sub>O<sub>3</sub> catalysts in the oxidation of CH<sub>3</sub>SSCH<sub>3</sub>.

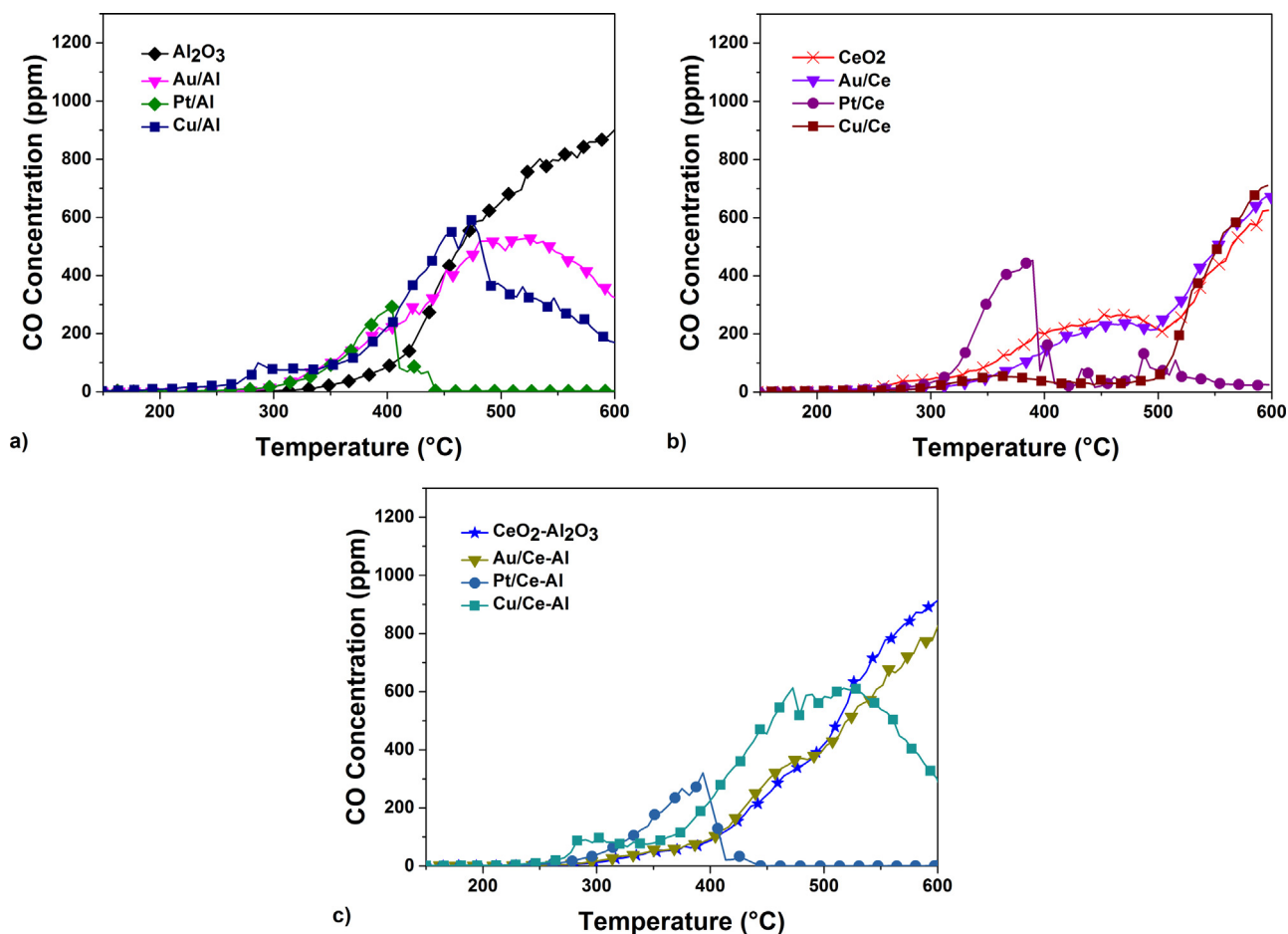


Fig. 10. CO concentration over (a) Au, Pt, and Cu on  $\gamma$ -Al<sub>2</sub>O<sub>3</sub>, (b) Au, Pt, and Cu on CeO<sub>2</sub>, as well as (c) Au, Pt, and Cu on CeO<sub>2</sub>-Al<sub>2</sub>O<sub>3</sub> catalysts in the oxidation of CH<sub>3</sub>SSCH<sub>3</sub>.

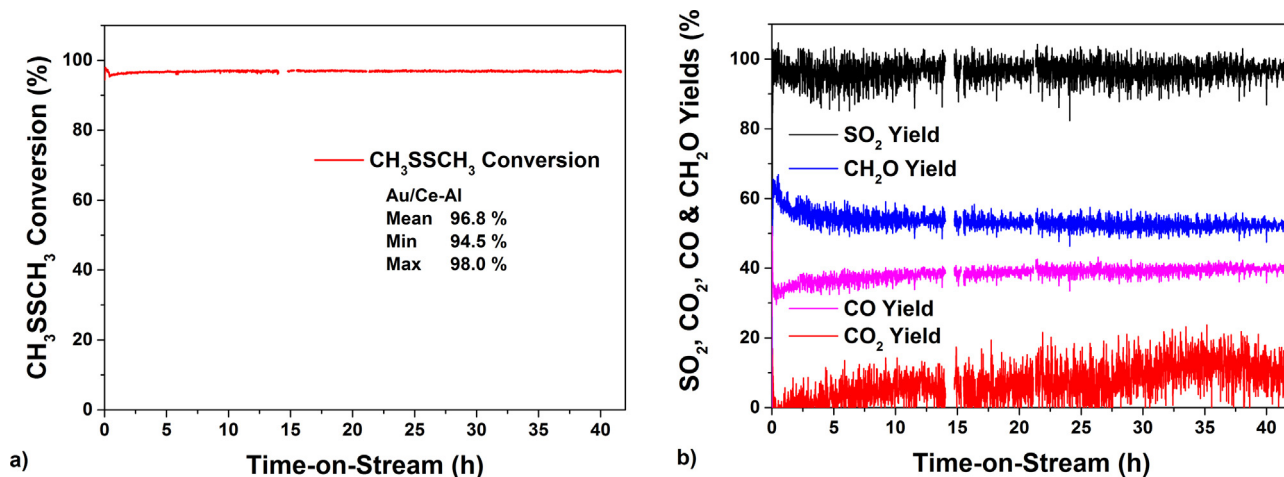


Fig. 11. Stability of the Au/Ce-Al catalyst in the CH<sub>3</sub>SSCH<sub>3</sub> oxidation during 41.6 h test (475 °C, 500 ppm of CH<sub>3</sub>SSCH<sub>3</sub>, WHSV 720 g gcat<sup>-1</sup> h<sup>-1</sup>).

and correspondingly a small increase in the CO<sub>2</sub> and CO formation were detected (Fig. 11b). The average yields of produced SO<sub>2</sub>, CO<sub>2</sub>, CO, and CH<sub>2</sub>O were 96.5%, 7.2%, 38.4%, and 53.3% throughout the test, respectively. The results indicate that the Au catalyst is a selective and stable catalyst in CH<sub>3</sub>SSCH<sub>3</sub> oxidation. This could be explained by the high electronegativity of Au, which makes it unreactive to other electronegative elements such as sulfur and oxygen [14,25]. However, it should be further modified to eliminate the formation of CH<sub>2</sub>O as well as CO instead of CO<sub>2</sub>.

#### 4. Conclusions

The objective of this study was to investigate the catalytic oxidation of CH<sub>3</sub>SSCH<sub>3</sub> over nine different supported catalysts (Au, Pt, and Cu). Pt and Cu were chosen as reference catalysts, because they have been used in previous research, both in academia and industry. The following observations are highlighted:

- Cu catalysts were interesting due to the substantially lower T<sub>50</sub> values. Au and Pt showed a better performance in the total SVOC

oxidation. Of these two catalysts Au catalysts could be better since Pt has a tendency to produce SO<sub>3</sub> that can further react with H<sub>2</sub>O, the active phase, and/or the support and consequently form sulfuric acid and/or metal salts, which may cause severe deactivation of the catalyst.

- Of all the catalysts, Cu/Ce-Al was the most active in terms of CH<sub>3</sub>SSCH<sub>3</sub> conversion and SO<sub>2</sub> formation, which started at lower temperature, as the activation of oxygen, which gave evidence that there is a connection between the activation of oxygen and CH<sub>3</sub>SSCH<sub>3</sub> reaction.
- The observed formation temperatures of SO<sub>2</sub> and CH<sub>2</sub>O were lower (~100 °C) compared to the oxygen activation temperatures which could be a result of CH<sub>3</sub>SSCH<sub>3</sub> reacting with the surface/bulk oxygen of the catalyst. Reducibility correlated with the formation of these two products over the Cu containing catalysts.
- No substantial decrease in the catalyst performance was detected in a stability test of 41.6 h at 475 °C over the Au/Ce-Al catalyst.

Considering further investigations, the shape and size of the Au nanoparticles would be important to determine in order to find structure-sensitivity of the catalysts in addition to the effects of the catalyst support on nanoparticles (SMSI). Since the reducibility of the catalyst seems to play an important role in the performance of the catalyst, a study on the oxidation state of the materials using XPS would be interesting. The combination of advantageous properties, *i.e.*, activity and sulfur resistance, is worth of further examinations. The preparation of bimetallic catalysts is of great interest.

## Acknowledgements

The work was done with the funding of the Council of Oulu region from the European Regional Development Fund (A32164), the City of Oulu, and Maj and Tor Nessling Foundation. Walter Ahlström Foundation, TES Foundation, and the University of Oulu Graduate School are appreciated for the support of this research. The research leading to these results has received funding also from the European Union Seventh Framework Programme [FP7/2007–2013] under grant agreement no. [PIRSES-GA-2012-317714]. Prof. Shudong Wang and Prof. Sheng Wang are highly appreciated for the use of HR-TEM at the Dalian Institute of Chemical Physics. Dr. Sandrine Arrii-Clacens, Mr. Jean-Dominique Comparot, Dr. Nelly Herauld, Dr. Henri-Joël Sedjame, and Mr. Mathias Barreau from the University of Poitiers are acknowledged for their assistance in the experimental work.

## References

- [1] Council Directive 1999/13/EC of 11 March 1999 on the limitation of emissions of volatile organic compounds due to the use of organic solvents in certain activities and installations, OJ L, 1999, 85, 42.
- [2] Council Directive 2010/75/EC of 24 November 2010 on industrial emissions (integrated pollution prevention and control), OJ L, 2010, 334, 53.
- [3] UNECE Consolidated text on the amended Protocol to the 1979 Convention on Long-range Transboundary Air Pollution to Abate Acidification, Eutrophication and Ground-Level Ozone, 2012, 28–29.
- [4] B. Halevi, J.M. Vohs, *J. Phys. Chem. B* 109 (2005) 23976–23982.
- [5] H. Chu, W.T. Lee, *Sci. Total Environ.* 209 (1998) 217–224.
- [6] H.V. Drushel, *The Analytical Chemistry of Sulfur and Its Compounds. Part II*, in: J.H. Karchmer (Ed.), John Wiley & Sons, New York, 1972, pp. 4–10.
- [7] M.J. Cardone, *The Analytical Chemistry of Sulfur and Its Compounds. Part II*, in: J.H. Karchmer (Ed.), John Wiley & Sons, New York, 1972, pp. 100–103.
- [8] S. Ojala, S. Pitkääho, T. Laitinen, N. Niskala Koivikko, R. Brahmi, J. Gaállová, L. Matejova, A. Kucherov, S. Päiväranta, C. Hirschmann, T. Nevanperä, M. Riihimäki, M. Pirilä, R.L. Keiski, *Top Catal.* 54 (2011) 1224–1256.
- [9] C. Hwang, N. Tai, *Appl. Catal. A* 393 (2011) 251–256.
- [10] H. Chu, G.H. Hao, T.K. Tseng, *Hazard. Mater.* 100 (2003) 301–316.
- [11] C. Wang, H. Weng, *Ind. Eng. Chem. Res.* 36 (1997) 2537–2542.
- [12] C. Wang, C. Lee, H. Weng, *Ind. Eng. Chem. Res.* 37 (1998) 1774–1780.
- [13] C. Wang, S. Lin, S. Liou, H. Weng, *Chemosphere* 49 (2002) 389–394.
- [14] J.A. Rodriguez, *Prog. Surf. Sci.* 81 (2006) 141–189.
- [15] J.-R. Chang, S.-L. Chang, T.-B. Lin, *J. Catal.* 169 (1997) 338–346.
- [16] A.K. Dalai, E.L. Tollefson, A. Yang, E. Sasaoka, *Ind. Eng. Chem. Res.* 36 (1997) 4726–4733.
- [17] V. Meeyoo, D.L. Trimm, N.W. Cant, *Appl. Catal. B* 16 (1998) L101–L104.
- [18] H. Chu, W.T. Lee, K.H. Horng, T.K. Tseng, *J. Hazard. Mater.* 82 (2001) 43–53.
- [19] J.M. Jones, V.A. Dupont, R. Brydson, D.J. Fullerton, N.S. Nasri, A.B. Ross, A.V.K. Westwood, *Catal. Today* 81 (2003) 589–601.
- [20] S. Bashkova, A. Bagreev, T.J. Bandosz, *Catal. Today* 99 (2005) 323–328.
- [21] C.F. Cullis, L.C. Roselaar, *Trans. Faraday Soc.* 55 (1959) 272–279.
- [22] C.F. Cullis, L.C. Roselaar, *Trans. Faraday Soc.* 55 (1959) 1562–1564.
- [23] S. Ojala, Ph.D. Thesis, University of Oulu, 2005, 2015.
- [24] J.R. Kastner, K.C. Das, Q. Buquoi, N.D. Melear, *Environ. Sci. Technol.* 37 (2003) 2568–2574.
- [25] G.C. Bond, *Catal. Rev. Sci. Eng.* 41 (1999) 319–388.
- [26] M. Haruta, *CATTECH* 6 (2002) 102–115.
- [27] M. Haruta, A. Ueda, S. Tsubota, R.M. Torres Sanchez, *Catal. Today* 29 (1996) 443–447.
- [28] M. Haruta, *Catal. Today* 36 (1997) 153–166.
- [29] D. Thompson, *Gold Bull.* 32 (1999) 12–19.
- [30] A.P. Kozlov, A.I. Kozlov, S. Sugiyama, Y. Matsui, K. Asakura, Y. Iwasawa, *J. Catal.* 181 (1999) 37–48.
- [31] L. Ilieva, P. Petrova, T. Tabakova, R. Zanella, M.V. Abrashev, J.W. Sobczak, W. Lisowski, Z. Kaszkur, D. Andreeva, *Catal. Today* 187 (2012) 30–38.
- [32] A.V. Kucherov, O.P. Tkachenko, O.A. Kirichenko, G.I. Kapustin, I.V. Mishin, K.V. Klementiev, S. Ojala, L.M. Kustov, R.L. Keiski, *Top Catal.* 52 (2009) 351–358.
- [33] A.V. Kucherov, I.M. Sinev, S. Ojala, R. Keiski, L.M. Kustov, *Stud. Surf. Sci. Catal.* 170 (2007) 1129–1136.
- [34] S. Ojala, J. Mikkola, R.L. Keiski, *Clean Air Research at the University of Oulu*, in: E. Pongrácz, M. Hyvärinen, S. Pitkääho, R.L. Keiski (Eds.), Kalevaprint, Oulu, 2010, pp. 50–53.
- [35] P. Lakshmanan, L. Delannoy, V. Richard, C. Méthivier, C. Potvin, C. Louis, *Appl. Catal. B* 96 (2010) 117–125.
- [36] R. Zanella, S. Giorgio, C.R. Henry, C. Louis, *J. Phys. Chem. B* 106 (2002) 7634–7642.
- [37] D. Martin, D. Duprez, *J. Phys. Chem.* 100 (1996) 9429–9438.
- [38] R.J.H. Grisel, P.J. Kooyman, B.E. Nieuwenhuys, *J. Catal.* 191 (2000) 430–437.
- [39] Z. Tang, J.K. Edwards, J.K. Bartley, S.H. Taylor, A.F. Carley, A.A. Herzing, C.J. Kiely, G.J. Hutchings, *J. Catal.* 249 (2007) 208–219.
- [40] B.L. Moroz, P.A. Pyraev, V.I. Zaikovskii, V.I. Bukhtiyarov, *Catal. Today* 144 (2009) 292–305.
- [41] S. Ivanova, C. Petit, V. Pitchon, *Appl. Catal. A* 267 (2004) 191–201.
- [42] S. Scirè, S. Minicò, C. Crisafulli, C. Satriano, A. Pistone, *Appl. Catal. B* 40 (2003) 43–49.
- [43] U.R. Pillai, S. Deevi, *Appl. Catal. A* 299 (2006) 266–273.
- [44] B.E. Solsona, T. Garcia, C. Jones, S.H. Taylor, A.F. Carley, G.J. Hutchings, *Appl. Catal. A* 312 (2006) 67–76.
- [45] X. Liu, P. Guo, B. Wang, Z. Jiang, Y. Pei, K. Fan, M. Qiao, *J. Catal.* 300 (2013) 152–162.
- [46] Q. Fu, A. Weber, M. Flytzani-Stephanopoulos, *Catal. Lett.* 77 (2001) 87–95.
- [47] F. Arena, P. Famulari, N. Interdonato, G. Bonura, F. Frusteri, L. Spadaro, *Catal. Today* 116 (2006) 384–390.
- [48] B. Chen, C. Shi, M. Crocker, Y. Wang, A. Zhu, *Appl. Catal. B* 132–133 (2013) 245–255.
- [49] D. Andreeva, V. Idakiev, T. Tabakova, L. Ilieva, P. Falaras, A. Bourlinos, A. Travlos, *Catal. Today* 72 (2002) 51–57.
- [50] Z. Abbasi, M. Haghighi, E. Fatehifard, S. Saedy, J. Hazard. Mater. 186 (2011) 1445–1454.
- [51] S. Pitkääho, L. Matejova, K. Jiratova, S. Ojala, R.L. Keiski, *Appl. Catal. B* 126 (2012) 215–224.
- [52] W. Dow, Y. Wang, T. Huang, *J. Catal.* 160 (1996) 155–170.
- [53] S. Zhang, W. Huang, X. Qiu, B. Li, X. Zheng, S. Wu, *Catal. Lett.* 80 (2002) 41–46.
- [54] L. Kundakovic, M. Flytzani-Stephanopoulos, *Appl. Catal. A* 171 (1998) 13–29.
- [55] D. Duprez, *Isotopes in Heterogeneous Catalysis*, in: J.S.J. Hargreaves, S.D. Jackson, G. Webb (Eds.), Imperial College Press, London, 2006, pp. 157–158, Chapter 6.
- [56] J.K. Edwards, B.E. Solsona, P. Landon, A.F. Carley, A. Herzing, C.J. Kiely, G.J. Hutchings, *J. Catal.* 236 (2005) 69–79.
- [57] G. Corro, A. Velasco, R. Montiel, *Catal. Commun.* 2 (2001) 369–374.
- [58] M. Waqif, P. Bazin, O. Saur, J.C. Lavalley, G. Blanchard, O. Touret, *Appl. Catal. B* 11 (1997) 193–205.
- [59] M. Waqif, A. Pieplu, O. Saur, J.C. Lavalley, G. Blanchard, *Solid State Ion.* 95 (1997) 163–167.
- [60] S.S. Deshmukh, M. Zhang, V.I. Kovalchuk, J.L. d'Itri, *Appl. Catal. B* 45 (2003) 135–145.
- [61] L. Kylhammar, P.-A. Carlsson, H. Härelind Ingelsten, H. Grönbeck, M. Skoglundh, *Appl. Catal. B* 84 (2008) 268–276.
- [62] M. Happel, L. Kylhammar, P.-A. Carlsson, J. Libuda, H. Grönbeck, M. Skoglundh, *Appl. Catal. B* 91 (2009) 679–682.
- [63] R.G. Nuzzo, D.L. Allara, *J. Am. Chem. Soc.* 105 (1983) 4481–4483.
- [64] R.G. Nuzzo, F.A. Fusco, D.L. Allara, *J. Am. Chem. Soc.* 109 (1987) 2358–2368.
- [65] R.G. Nuzzo, B.R. Zegarski, L.H. Dubois, *J. Am. Chem. Soc.* 109 (1987) 733–740.
- [66] C.D. Bain, E.B. Troughton, Y.T. Tao, J. Evall, G.M. Whitesides, R.G. Nuzzo, *J. Am. Chem. Soc.* 111 (1989) 321–335.